The Linear Sensitivity of the North Atlantic Oscillation and Eddy-Driven Jet to SSTs

HUGH S. BAKER AND TIM WOOLLINGS

Atmospheric, Oceanic and Planetary Physics, University of Oxford, Oxford, United Kingdom

CHRIS E. FOREST

Department of Meteorology and Atmospheric Science, and Department of Geosciences, Earth and Environmental Systems Institute, The Pennsylvania State University, University Park, Pennsylvania

MYLES R. ALLEN

Atmospheric, Oceanic and Planetary Physics, and School of Geography and the Environment, University of Oxford, Oxford, United Kingdom

(Manuscript received 14 January 2019, in final form 2 July 2019)

ABSTRACT

The North Atlantic Oscillation (NAO) and eddy-driven jet contain a forced component arising from sea surface temperature (SST) variations. Due to large amounts of internal variability, it is not trivial to determine where and to what extent SSTs force the NAO and jet. A linear statistical–dynamic method is employed with a large climate ensemble to compute the sensitivities of the winter and summer NAO and jet speed and latitude to the SSTs. Key regions of sensitivity are identified in the Indian and Pacific basins, and the North Atlantic tripole. Using the sensitivity maps and a long observational SST dataset, skillful reconstructions of the NAO and jet time series are made. The ability to skillfully forecast both the winter and summer NAO using only SST anomalies is also demonstrated. The linear approach used here allows precise attribution of model forecast signals to SSTs in particular regions. Skill comes from the Atlantic and Pacific basins on short lead times, while the Indian Ocean SSTs may contribute to the longer-term NAO trend. However, despite the region of high sensitivity in the Indian Ocean, SSTs here do not provide significant skill on interannual time scales, which highlights the limitations of the imposed SST approach. Given the impact of the NAO and jet on Northern Hemisphere weather and climate, these results provide useful information that could be used for improved attribution and forecasting.

1. Introduction

The North Atlantic Oscillation (NAO) is a teleconnection pattern that dominates the climate variability over the North Atlantic (Wallace and Gutzler 1981; Hurrell 1995). Partly resulting from the internal variability of midlatitude dynamics, it is also externally driven (e.g., Hurrell et al. 2013). Sea surface temperatures (SSTs) in many different locations have been shown to be important external NAO drivers (e.g., Rodwell et al. 1999; Hoerling et al. 2001; Czaja and Frankignoul 2002; Peng et al. 2002; Bader and Latif 2003; Wang et al. 2004; Kucharski et al. 2006). However, due to internal variability and signal-to-noise issues, one requires either long observational datasets or large climate ensembles to say with confidence where and to what extent SSTs are responsible for forcing the NAO.

There have been numerous studies investigating the winter NAO response to SST forcing. The recent warming

Denotes content that is immediately available upon publication as open access.

Supplemental information related to this paper is available at the Journals Online website: https://doi.org/10.1175/JCLI-D-19-0038.s1.

Corresponding author: Hugh S. Baker, hugh.baker@physics.ox.ac.uk

DOI: 10.1175/JCLI-D-19-0038.1

trend in the Indian Ocean has been shown to force a positive NAO (Hoerling et al. 2001, 2014; Bader and Latif 2003, 2005). While there were concerns about spurious results arising from missing ocean–atmosphere coupling leading to incorrect sea level pressure (SLP) in these studies (Copsey et al. 2006), Colfescu et al. (2013) showed that the incorrect SLP may in fact arise from model bias, thus not ruling out the Indian Ocean–NAO link. Further to this, Fletcher and Cassou (2015) also demonstrate the link using a coupled model. The mechanism postulated is the generation of a Rossby wave from the SST warming, which constructively interferes with a climatological stationary wave, thus forcing a positive NAO response (Fletcher and Kushner 2011). However, the simulated NAO trend amplitude underestimates the observed trend, suggesting that other drivers may also be important (King et al. 2010). The Atlantic tripole SST pattern has also been shown to force the NAO (Rodwell et al. 1999; Czaja and Frankignoul 2002; Peng et al. 2002; Wang et al. 2004), although the tripole pattern in the SSTs can also be considered as a combined SST–atmospheric response (Cassou et al. 2007). Further to this, the Pacific has also been linked to forcing the NAO (Kucharski et al. 2006; Fletcher and Kushner 2011). These numerous studies employ a range of methodologies to find the links between SSTs and the winter NAO, which makes it hard to compare and identify the SST forcing importance in each location. In contrast, there are only a handful of studies looking at the summer NAO (SNAO) response to SSTs, which indicate some connection to the Atlantic multidecadal variability (Folland et al. 2009; Sutton and Dong 2012). However, given that the SNAO is the dominant pattern of variability in the North Atlantic (Folland et al. 2009; Bladé et al. 2012), a systematic study of the SNAO sensitivity to SSTs would provide useful information for predicting and attributing particular SNAO phases.

Skillfully predicting the winter NAO has, until recently, proved elusive (Scaife et al. 2014), due to climate models showing little response to slowly varying climate system components such as the ocean (Kushnir et al. 2006). Recently, high predictability of the winter NAO has been observed using the Met Office Global Seasonal forecast System 5 (Scaife et al. 2014). A portion of this skill is shown to come from North Atlantic SSTs (Smith et al. 2016). Using a global sensitivity map of the NAO to SSTs, it is possible to reconstruct the winter NAO time series (Li and Forest 2014) and investigate if there is any skill in reconstructing and forecasting the NAO, and if so, where it comes from. To date, no skill has been reported for predicting the SNAO in seasonal forecast systems (Dunstone et al. 2018).

Early studies computed the sensitivity of atmospheric variables to SSTs using a Green's function approach via the systematic application of patches across the ocean domains (Barsugli and Sardeshmukh 2002; Barsugli et al. 2006). However, later work (Li et al. 2012; Li and Forest 2014), used a random perturbation method (RPM), whereby random SST fields are generated with anomalies across the ocean domain. The two methods give consistent sensitivity information and similar reconstruction of the regional response (Li et al. 2012). However, the RPM method is about 12 times more computationally efficient than the patch method due mainly to the larger area-integrated SST forcing amplitude.

Here we employ the method used in Li and Forest (2014), who used it to investigate the sensitivity of the winter NAO to SSTs with 200-member ensembles. We use a 5000-member ensemble to investigate both the winter NAO and SNAO sensitivities to SST forcing, and explore the mechanisms behind the sensitivities for the first time in this framework. We also investigate the eddy-driven jet sensitivity to SSTs, as the jet is intimately linked to the NAO. We then use these sensitivities to reconstruct NAO and jet index time series, and explore where the skill in these reconstructions comes from. We also use these sensitivities to apply a novel approach to forecasting the NAO and SNAO.

Section 2 describes the reanalysis data used, how the ensemble simulations are designed, and how the linear statistical–dynamic method works. In section 3 we present our findings, along with a discussion of the results in the context of previous studies and some of the limitations of our method, before concluding in section 4.

2. Methods

a. *Reanalysis datasets*

Throughout this study, we make use of three reanalysis datasets to compare to and validate our model results. These are: the NOAA-CIRES Twentieth-Century Reanalysis, (NOAA-20C; Compo et al. 2011), the Twentieth-Century ECMWF Re-Analysis (ERA-20C; Poli et al. 2016), and the NCEP–DOE Reanalysis 2 (NCEP2; Kanamitsu et al. 2002). NAO time series for each reanalysis are computed by projecting each individual season onto the first EOF of the reanalysis SLP for that particular season (e.g., the ERA-20C winter NAO time series is computed by projecting the December–February (DJF) mean SLP for each year onto the first EOF of the DJF ERA-20C SLP) The NAO EOF is computed over the region 20°–80°N, 90°W–40°E). Throughout the study we use standardized NAO indices, and refer to winter as the DJF period and summer as the June–August (JJA) period.

b. Random perturbation method ensemble

We make the assumption that the large-scale atmosphere responds to SST forcing with a linear component. Following Li et al. (2012), the relationship between forcing and response can then be represented as a continuous Green's function:

$$\Delta R \approx \int G(x')\,\Delta\mathrm{SST}(x')\,dA\,, \tag{1}$$

where ΔR is the atmospheric response anomaly, $\Delta\mathrm{SST}(x')$ is the related SST anomaly located at x' with area dA, and G is a linear operator. This linear operator, the global teleconnection operator (GTO), is a set of sensitivities describing the atmospheric response to SST forcing at each grid point.

To allow us to compute the GTO, we use a large ensemble of perturbed SST runs. We use the RPM to generate an ensemble of SST perturbation fields as described in Li et al. (2012). Following Li et al. (2012), each random perturbation field is created as a 16×16 matrix, with each point having a temperature value randomly drawn from a uniform temperature distribution between -2 and 2 K. The matrix is then bilinearly interpolated onto a grid with N96 resolution (145 latitude points $\times$ 192 longitude points). To ensure local maxima and minima do not just occur on the original 16×16 grid, we shift each initial coordinate randomly by 0–8 grid points zonally and 0–5 grid points meridionally.

We generate 5000 SST perturbation fields and add them to the 1980–99 climatological monthly SSTs in the merged Hadley–NOAA optimum interpolation (OI) SST dataset (Hurrell et al. 2008) to create a 5000-member ensemble. Perturbation fields are applied between 60°N and 60°S, and to ensure a smooth decrease at the boundaries, we weight the perturbations between 50° and 60° (both north and south) with linearly decreasing weights from 0.9 to 0.1.

We use the HadAM3P model to run the ensemble. HadAM3P is an atmosphere only, medium resolution (run here at N96 resolution, or 1.25° $\times$ 1.875°), GCM developed by the Met Office. It is based upon the atmospheric component of HadCM3 (Pope et al. 2000; Gordon et al. 2000). The model has 19 hybrid (sigma levels near the surface, changing smoothly to pressure levels near the top of the atmosphere) vertical levels (Simmons and Burridge 1981), with six levels above 200 hPa, the highest of these just above 5 hPa. We use an improved version of HadAM3P that has a more sophisticated land surface scheme (Guillod et al. 2017). We run HadAM3P using the large-ensemble capability provided by the climateprediction.net volunteer computing network (Allen 1999; Guillod et al. 2017), where members of the public run initial condition ensemble GCM simulations. The HadAM3P representations of many midlatitude Northern Hemisphere winter circulation features, including the trimodal Atlantic eddy-driven jet structure, the Atlantic storm track, and Atlantic blocking, have been shown to be better than the majority of models in the Coupled Model Intercomparison Project and associated atmosphere-only models (Mitchell et al. 2017). The 850-hPa zonal wind biases are shown in Fig. S1 in the online supplemental material, showing that in winter and summer the model North Atlantic jet biases are small. Biases are also small in the other midlatitude regions, suggesting the model should simulate teleconnections well too due to a low waveguide bias. The ability of HadAM3P to capture these dynamical phenomena well makes it a good model choice for assessing the midlatitude circulation sensitivity to SSTs.

For each ensemble member we run a control simulation and forced simulation. The control simulation is run for 25 months (December 1998–December 2000), and uses the 1980–99 Hadley–NOAA OI climatological mean monthly SSTs, and observed greenhouse gas forcings from 1998 to 2000. The forced simulation is exactly the same, but with the SST perturbation applied, giving 5000 control and forced ensemble member pairings. Each pairing also has an initial condition perturbation via perturbations to the potential temperature (which is the same for both runs in the pair), for full details see Massey et al. (2015). We discard the first year of each simulation, giving us one winter and one summer season for each ensemble member. We define each ensemble member response as the difference between each forced and control ensemble member pair.

c. The GTO and linear reconstructions

Following Li et al. (2012), we compute the GTO for a particular atmospheric response variable by employing a linear regression between the seasonal atmospheric anomaly and the SST anomalies:

$$R = G\,\Delta\mathrm{SST} + e\,, \tag{2}$$

where e is the error related to the nonlinearity and the internal noise. Using the result derived in the appendix of Li et al. (2012), the smoothed GTO estimate is given by

$$G(\mathbf{x}_i) = \frac{\mathrm{Cov}[\Delta\mathrm{SST}_n(\mathbf{x}_i), \mathbf{R}_n]}{\frac{T_{\max}^2}{3} L_x L_y} + e\,, \tag{3}$$

where G is computed at each grid point $\mathbf{x}_i$. The term $\Delta\mathrm{SST}_n(\mathbf{x}_i)$ is a vector of the 5000 time-independent SST

perturbation anomalies (as described in section 2b above) at the grid point $\mathbf{x}_i$, $\mathbf{R}_n$ is a vector of the 5000 atmospheric anomaly indices, $T_{\max} = 2\,\mathrm{K}$, the maximum SST perturbation, and $L_x = a\lambda_0 \cos(\phi_i)$ and $L_y = a\phi_0$ are the RPM lattice local length scales (a is Earth's radius, ϕ_0 and λ_0 are the latitude and longitude gridpoint spacings in radians, and ϕ_i is the latitude of the grid point for which G is being computed for).

Once the GTO has been obtained, it can be used to reconstruct the response of an atmospheric variable to a particular SST field. This is achieved by projecting the SST field onto the GTO:

$$\Delta R = \gamma \sum_{\mathbf{x}_i} G(\mathbf{x}_i)\, \Delta T_{\mathrm{SST}}(\mathbf{x}_i) L_x L_y, \tag{4}$$

where ΔT_{SST} refers to the SST anomaly of the particular SST field one wishes to reconstruct the atmospheric response to. By repeatedly performing the reconstruction process for a time series of SST fields, we can create a reconstructed time series of ΔR. The coefficient γ depends on the length scales of both the forcing and response for a given target response based on the dynamics (Li et al. 2012). Although the scaling by the γ coefficient does not affect correlation results between reconstructed and reanalysis time series, it is insightful to be able to investigate the size of the signal of the reconstructed response. To scale the reconstructed response to have physical meaning, we perform a simple linear regression of the reconstructed time series onto the NOAA-20C reanalysis time series for each variable. The reconstructed time series is then scaled by the regression coefficients, that is:

$$R_{\mathrm{scaled}} = \alpha R_{\mathrm{reconstructed}} + \beta, \tag{5}$$

where α and β are the regression coefficients determined by the regression $R_{\mathrm{reanalysis}} = \alpha R_{\mathrm{reconstructed}} + \beta$. As the reanalysis time series has been standardized, this means that the scaled time series has a standard deviation equal to the correlation between the reconstructed time series and the NOAA-20C reanalysis time series.

For this study we investigate the GTO for the NAO and North Atlantic eddy-driven jet. For each ensemble member pair, we define response NAO and jet indices. The response NAO for each member is defined by the difference of the normalized projections of the forced and control seasonal mean SLP fields onto the first model EOF of SLP over 20°–80°N, 90°W–40°E. This gives a standardized response index. The model and reanalysis EOFs are shown in Figs. S2 and S3 for winter and summer, respectively. The pattern correlations between any two given EOFs in a particular season are all greater than 0.9, and using the model EOF or a reanalysis EOF does not significantly affect the calculation of the GTO (not shown). The jet speed and latitude responses are taken as the difference between the forced and control indices as defined using the jet indices in Woollings et al. (2010), defined over 15°–75°N, 60°W–0°. We use daily data at 850 hPa to compute the jet indices, and then compute the mean index for each season before taking the difference to compute the response.

To reconstruct long time series of the NAO and jet indices from the GTO, we use the HadISST dataset (Rayner et al. 2003). We project the monthly SSTs from the dataset onto the GTO and then take the mean across each season to define a reconstructed index for a particular year (e.g., to compute the SNAO for a particular year, we project June, July, and August SSTs separately onto the SNAO GTO, then take the mean of the three projections to get the reconstructed SNAO for that year).

3. Results and discussion

a. *The North Atlantic Oscillation*

Figure 1 shows the GTO for the NAO in winter and summer. The maps display the NAO sensitivity to anomalous SSTs. For example, the winter NAO exhibits a positive response to anomalous warming over the Indian Ocean. The winter GTO bears strong resemblance to the winter GTOs computed for the CAM5 and GFDL models, shown in Fig. 3 of Li and Forest (2014). It is worth noting that Li and Forest (2014) use 200-member ensembles to compute their GTOs, and so there are fewer regions of statistical significance compared to the HadAM3P GTO. The strong region of winter NAO sensitivity to Indian Ocean SSTs corroborates previous studies linking the warming trend in Indian Ocean SSTs and the positive NAO trend from 1950 to 2000 (e.g., Hoerling et al. 2001, 2004; Bader and Latif 2003, 2005).

The winter NAO also appears sensitive to an SST dipole in the tropical Pacific, and a tripole pattern in the North Atlantic. Kucharski et al. (2006) link a Pacific dipole pattern to the winter NAO; however, their dipole pattern consists of warm SSTs in the tropics and cooler SSTs in the northern subtropics. There are several reasons why a discrepancy may arise between this study and their work. The GTO only picks out the linear sensitivity to SSTs; the GTO is constructed so that it captures the response to an anomalous SST pattern throughout the year and so does not provide any temporal information about when the NAO is sensitive to the SSTs (i.e., it may be the October SSTs in the Pacific that are important for forcing the winter NAO. This will be investigated later in the study). Kucharski et al. (2006) find the link

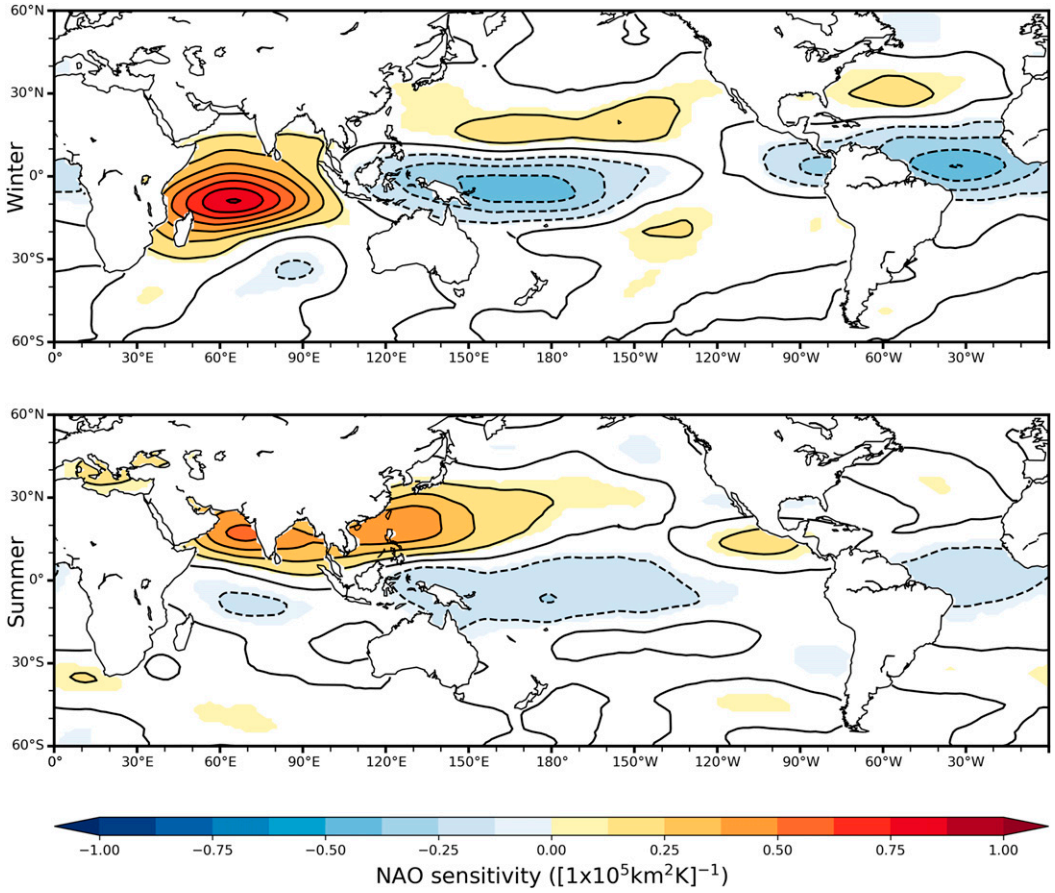

FIG. 1. Sensitivity of the NAO index to SST anomalies given by the $G(x')$ in Eq. (1). Shaded regions indicate statistical significance at the 5% level using a two-tailed t test.

between the low-frequency variability in the Pacific and the NAO.

The North Atlantic tripole pattern has also been studied and found to be associated with the winter NAO (e.g., Rodwell et al. 1999; Czaja and Frankignoul 2002; Peng et al. 2002; Wang et al. 2004). The GTO picks out the same sign of tripole pattern (cold–warm–cold) as in the literature that is associated with a positive NAO. On the question of causality between the SST anomalies and the NAO, the GTO method takes prescribed SST patterns and looks at their impact on the NAO. The sensitivity map given by the GTO therefore only includes information of the model response to SSTs, and does not take into account any influence from the atmosphere onto the SSTs (discussed in section 3c).

The SNAO also appears to be sensitive to SSTs, in similar regions to the winter NAO. The northern Indian Ocean and subtropical west Pacific are associated with a positive SNAO, while the southern Indian and tropical western Pacific are associated with a negative SNAO. The tripole pattern is also visible, except only the tropical Atlantic displays a statistically significant sensitivity region. In agreement with O'Reilly et al. (2018), there seems to be no strong El Niño–Southern Oscillation (ENSO) to SNAO relationship. The weaker, yet still statistically significant, sensitivity map for the SNAO suggests that there may be some skill in reconstructing the SNAO, something that has previously not been reported in any forecast systems (Dunstone et al. 2018).

Using Eqs. (4) and (5), we reconstruct winter NAO and SNAO time series from the HadISST dataset. Shown in Fig. 2 are the reanalysis and reconstructed time series, along with the correlation coefficients between each reanalysis time series and the reconstructed time series. The reconstructed winter NAO is significantly (at the 5% level using a two-tailed t test) correlated with all three reanalysis products, with a similar correlation coefficient of around 0.4 between the reconstruction and the NAO index from reanalysis as found by Li and Forest (2014). By construction, due to the scaling method applied in Eq. (5), the reconstructed

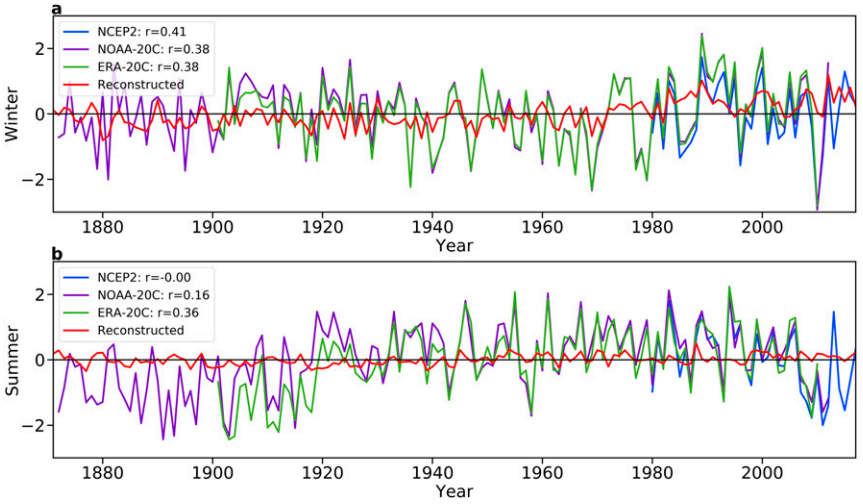

FIG. 2. Time series of the NAO in (a) winter and (b) summer. The reconstructed NAO time series is calculated using Eq. (4), and then scaled using Eq. (5). For winter, the year refers to the year in which January and February fall.

time series standard deviation is equal to the correlation with the NOAA-20C time series. As in Li and Forest (2014), the reconstructed time series captures the trend toward more positive NAO values later in the time series, suggesting this trend is forced by SSTs. This will be explored later in the study.

Only the ERA-20C time series is correlated significantly with the reconstructed SNAO. These differences in correlations are due to the different reanalyses spanning different time periods. Given the high correlation between the three reanalysis time series, this suggests that the teleconnection strength between the SSTs and the SNAO varies temporally. The reconstructed SNAO also fails to capture the trend in recent years to a more negative SNAO, suggesting this trend is not being forced, at least linearly, by changes in SSTs. The correlations suggest that in winter, SSTs explain around 20% of the variability of the NAO, while the lower correlations in summer suggest that a smaller portion of the SNAO variability is forced by the SSTs compared to the NAO (although in summer exactly how much variability explained by the SSTs depends on the time period considered).

Given the apparent varying reconstruction skill in summer, we proceed to calculate the correlations between the reanalysis and reconstructed NAO time series using a 31-yr moving window (shown in Fig. 3). We assess statistical significance at the 5% level using a two-tailed t test. Autocorrelation is accounted for following Wilks (2011) by using the lag-1 autocorrelation of the full NOAA-20C and reconstructed NAO time series to determine the effective sample size of the 31-yr period. In winter, the skill is fairly consistently around 0.4, with a statistically significant correlation between the reconstructed and reanalysis time series across much of the period. Interestingly, we do not observe the same level of drop-off in skill as seen by Weisheimer et al. (2017) in the 1950–70s, who use atmosphere-only hindcast experiments to investigate the skill in NAO forecasts. This could be due to intermodel differences in the teleconnection strength between SSTs and the NAO, or other processes simulated poorly in the atmosphere-only model that do not contribute in the GTO method. Our results are consistent with those of Kumar and Chen (2018), who also do not observe lower skill during the low-skill period in Weisheimer et al. (2017) when they investigate the skill in reproducing the Arctic Oscillation in AMIP simulations. The winter NAO skill using the GTO method is also consistently equal to or higher than that in Weisheimer et al. (2017). In summer, as mentioned earlier, the skill varies across the period. Before 1915, the skill is very poor, but then it rises through to 1925, remaining high until 1995, before declining again. The reason for this time varying skill will be explored later in the study. In this high-skill period, the correlation is statistically significant and consistently between 0.4 and 0.6. We believe that this high level of skill in reconstructing the SNAO has not been shown in any previous studies.

1) WINTER

In this section, we investigate the winter sensitivities, reconstructions, and forcing mechanisms in more detail. To gain an understanding of how SSTs force the NAO, there are two components to understand. The first, demonstrated by the GTO, is where and to what degree is the NAO sensitive to SSTs. The second component is to understand where SSTs are varying in these regions of sensitivity. We decompose the global oceans into three

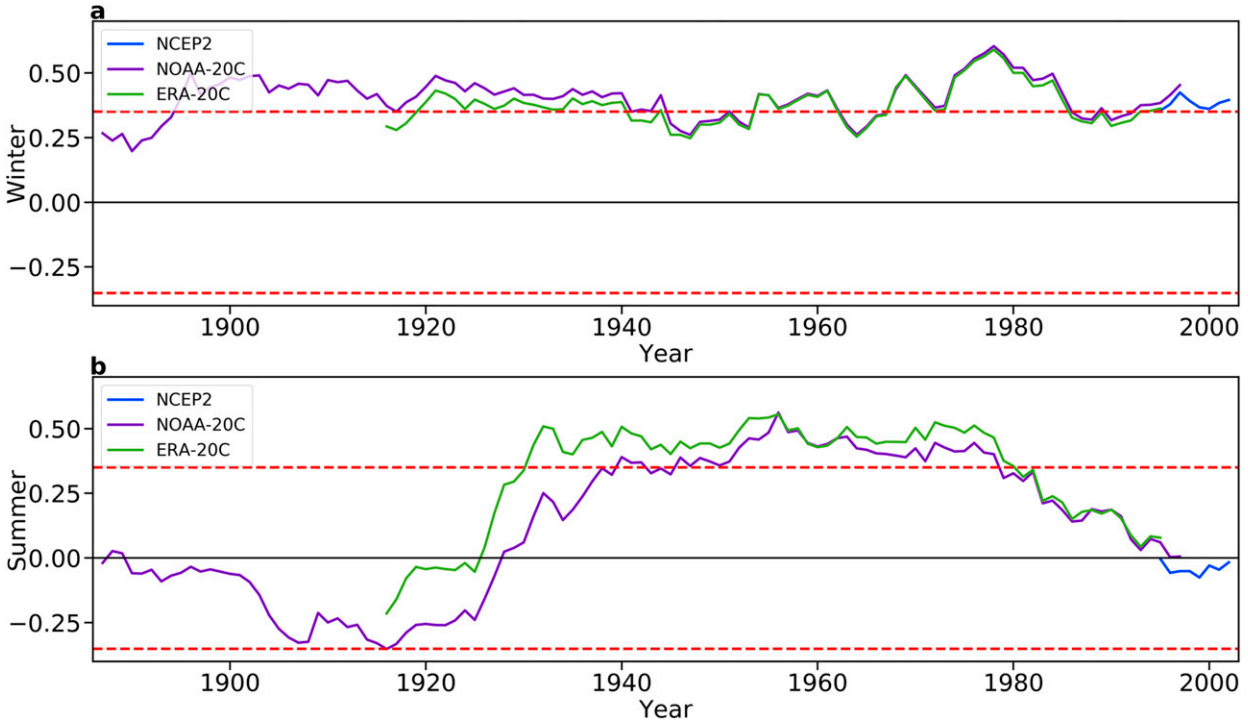

FIG. 3. The 31-yr moving correlation of the reconstructed NAO with the NAO times series from the reanalyses in (a) winter and (b) summer. The red dashed lines indicate statistical significance at the 5% level using a two-tailed *t* test. The year refers to the middle year of the 31-yr moving window.

regions: the Atlantic (90°W–30°E), the Indian Ocean (30°–110°E), and the Pacific (110°E–90°W). We then proceed to reconstruct the NAO using SSTs from each ocean in turn (shown in Fig. 4 for winter), using SSTs from 60°S to 60°N, the full latitudinal extent of the GTO. In winter, the Atlantic reconstruction captures the largest portion of the variance, with the Pacific also contributing. This supports the findings of Li and Forest

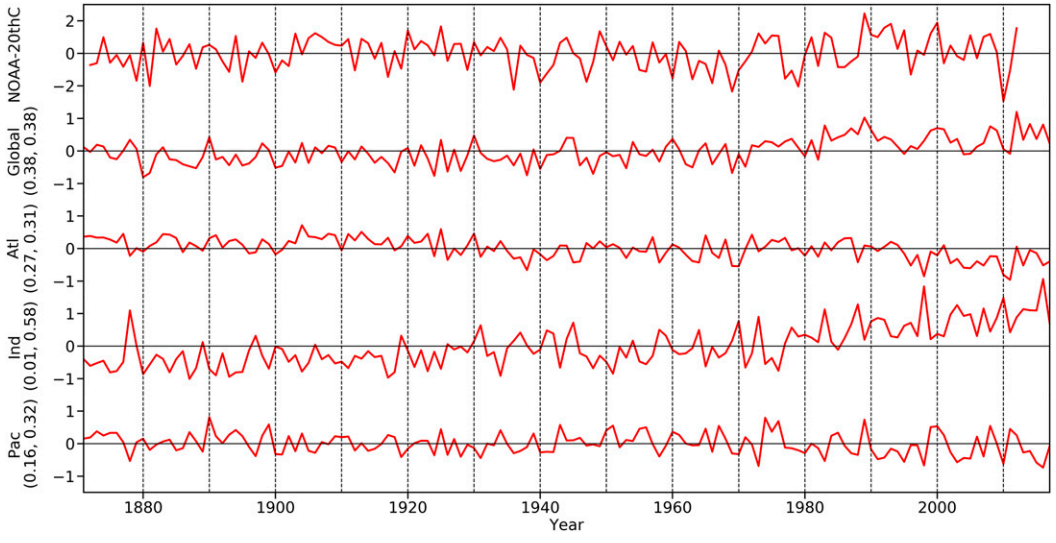

FIG. 4. NOAA-20C winter NAO time series and reconstructed NAO time series using different ocean basin winter SSTs. Global uses all SSTs, Atlantic uses 90°W–30°E, Indian uses 30°–110°E, and Pacific uses 110°E–90°W. The year refers to the year in which January and February fall. The numbers in parentheses indicate the correlation of the time series with the NOAA-20C NAO and the standard deviation of the time series.

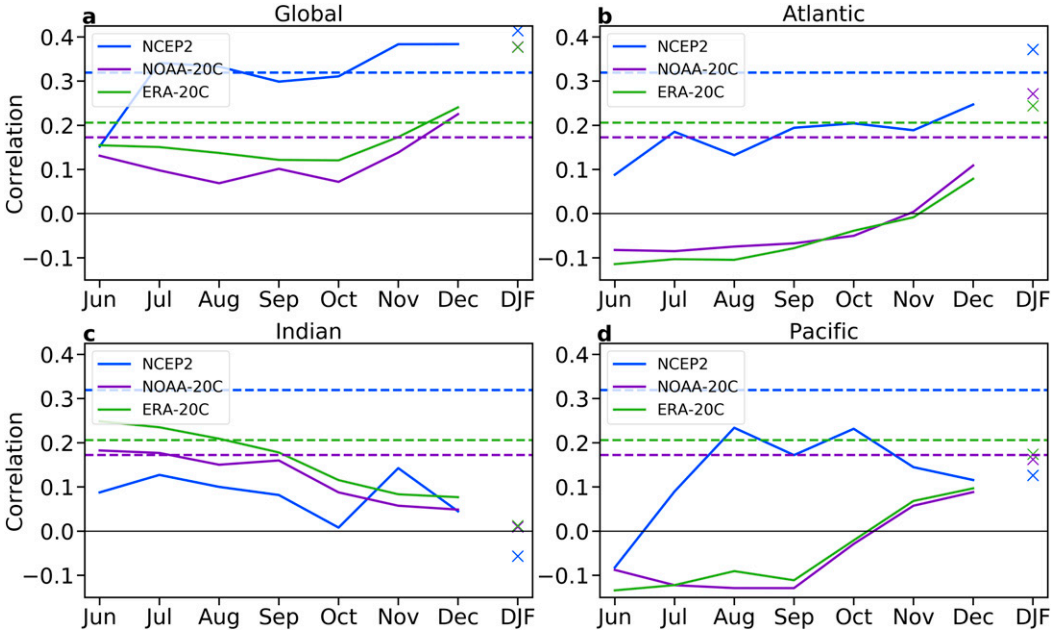

FIG. 5. Reconstructed time series correlated with reanalysis time series using SSTs (a) globally; (b) from the Atlantic basin, 90°W–30°E; (c) from the Indian basin, 30°–110°E; and (d) from the Pacific basin, 110°E–90°W. Along the abscissa are the individual months used to reconstruct the succeeding winter (DJF) NAO. The crosses mark the correlation of the reconstruction using the DJF SSTs with the reanalysis time series. The dashed lines mark the correlation required for the reconstruction and reanalysis to be correlated with a statistical significance at the 5% level, computed using a two-tailed *t* test.

(2014), who showed that SSTs from the Indian Ocean are not sufficient to skillfully reconstruct the NAO, and that SSTs from the tropical Pacific or Atlantic are needed to provide skill. Using the analysis, it is possible to see if the NAO in a particular year has some response that may be attributed to SST forcing, and also to look at which basin may have been important. For example, in 2010 the anomalously negative observed NAO appears to have been forced in some part by the Atlantic and Pacific SSTs. Interestingly, on the fast time scales, the Indian Ocean is not correlated with the reanalysis, even though the winter NAO has a large region of sensitivity to SSTs in the Indian Ocean, and the high standard deviation in the Indian Basin reconstruction suggests that there is variability in the Indian Ocean SSTs. The trend to more positive NAO years in the later part of the time period does appear to be linked to the Indian Ocean, but we cannot confirm this as the reconstruction has no skill coming from the Indian Ocean. The issue of the Indian Ocean will be discussed further in section 3c.

While Li and Forest (2014) investigated the NAO reconstruction skill using the GTO, it is also possible to use the method to forecast the NAO. Using preceding monthly SSTs, we reconstruct the winter NAO using SSTs in turn from individual months in the preceding year, up to the December in which the winter begins. We then correlate each reconstruction with the reanalysis time series. We do this for global SSTs and for each of the three basins. Figure 5 shows the results of these lagged reconstructions for all the months and basins. Autocorrelation is accounted for in the significance test by computing the effective sample size as before, this time using the minimum effective sample size across all basins and reconstruction month time series. As expected, the global reconstruction improves as the month used gets closer to the winter being reconstructed. We do not observe any skill arising from the previous winter SSTs (not shown) (cf. Dunstone et al. 2016). For the later period (NCEP2 reanalysis), the correlation is significant when using the November SSTs, indicating that there is some skill in forecasting the winter NAO. Decomposing this skill further into tropical versus midlatitude components gives a 0.40 correlation between the reconstruction using tropical November SSTs and the NCEP2 NAO versus a 0.01 correlation from using the midlatitude SSTs. This further validates the model, and the skill of preceding SSTs in forecasting the NAO shows that we are not just seeing a manifestation of false predictability arising from a lack of atmosphere–ocean coupling (cf. Bretherton and Battisti 2000, see also discussion in section 3c) as the skill is coming from remote tropical forcing and from SSTs in the month before the NAO is being reconstructed.

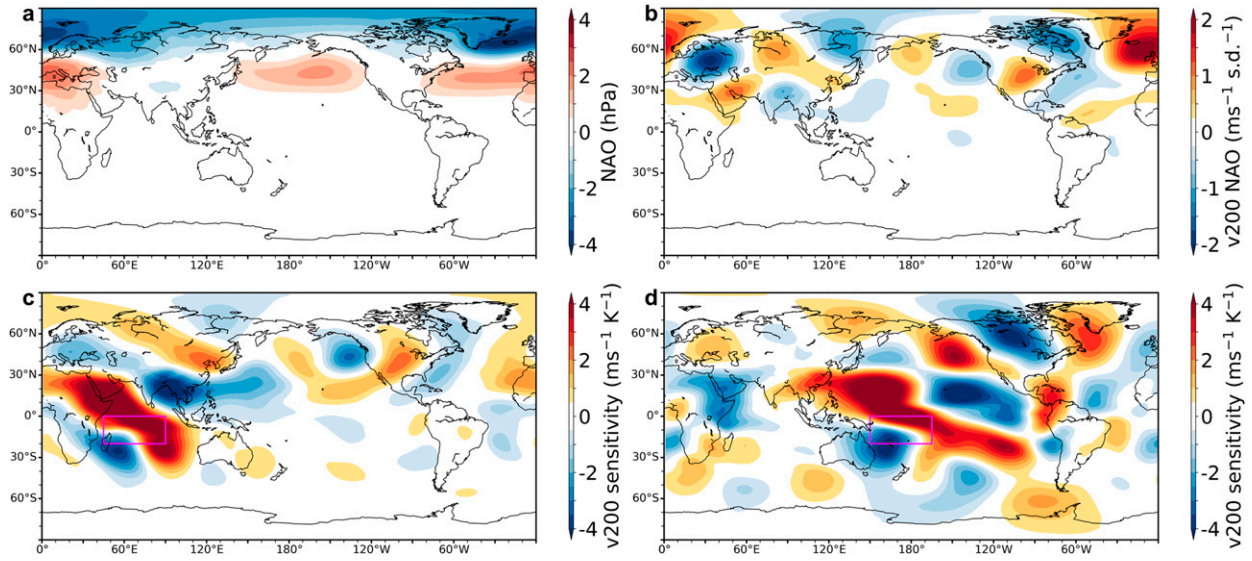

FIG. 6. (a) Control ensemble member winter SLP regressed onto principal components associated with the first EOF of winter SLP in HadAM3P (defined over the region 20°–80°N, 90°W–40°E). (b) The 200-hPa meridional wind from the HadAM3P control ensemble members regressed onto the ensemble member principal components of the first EOF. Regression of the 200-hPa meridional wind responses onto the SST perturbations averaged over the pink box computed for the (c) Indian Ocean SST box and (d) Pacific Ocean SST box.

The skill also increases toward the winter when using SSTs from the Atlantic basin, suggesting a fairly direct effect of the SSTs on the circulation such as due to changing temperature gradients or modifying eddy behavior. In contrast, the main skill in the Indian Ocean comes from SSTs earlier in the year, with some significant skill using June and July SSTs to forecast the winter NAO in ERA-20C and NOAA-20C (the lack of skill here in forecasting the NCEP2 NAO arises as the reanalyses cover different time periods). We note that these long-lead time scales should be treated with caution; while it appears the Indian Ocean SSTs may contribute to the trend in the NAO and this decadal signal may be what is being picked up as significant, the Indian Ocean SSTs do not seem to add any forecast skill for forecasting on interannual time scales (see discussion on Indian Ocean in section 3c). The Pacific SSTs in the later period seem to provide some skill in late summer/early autumn, but this is not statistically significant.

Despite the apparent lack of skill in the reconstruction and forecasting arising from the Indian Ocean, it is still insightful to consider how it forces the NAO in the model. The spatial separation and lag between the Indian Ocean SSTs forcing the winter NAO, and to a lesser extent the Pacific SSTs forcing the winter NAO, suggest that the forcing mechanism may manifest via Rossby waves. To investigate this we look for patterns in the 200-hPa meridional wind response in winter to Indian and Pacific SSTs. Figure 6a shows the control ensemble members SLP regressed onto the set of control ensemble member principal components associated with the first EOF of SLP in winter in HadAM3P (defined over the region 20°–80°N, 90°W–40°E). Figure 6b is the 200-hPa meridional wind at each grid point across the control ensemble members regressed onto the set of control ensemble member principal components of the model's first EOF. It shows that the winter NAO has a circumglobal wave train associated with it, which has a cyclonic region over Greenland, as expected for a positive NAO. This pattern is very similar to the pattern obtained by performing the same regression for the observed meridional wind and NAO (see Fig. S4). To investigate the circulation response to SSTs, we form an SST anomaly index given by the anomaly between a forced and control ensemble member pair, averaged over a particular region. We then regress the 200-hPa meridional wind anomalies onto the SST anomalies. Figure 6c shows the meridional wind response to SSTs over the region of high winter NAO sensitivity in the Indian Ocean (pink box). The local response exhibits the classical quadrupole structure (e.g., Jin and Hoskins 1995); however, there is also a midlatitude wave response that propagates eastward into the Atlantic basin. The wavenumber and phase of this wave match the wave associated with the model EOF, particularly over the western Pacific, North America and into the Atlantic region. This provides evidence for a Rossby wave–like forcing of the winter NAO from the Indian Ocean. The Pacific response (Fig. 6d) also features a wave train propagating over North America and into the Atlantic,

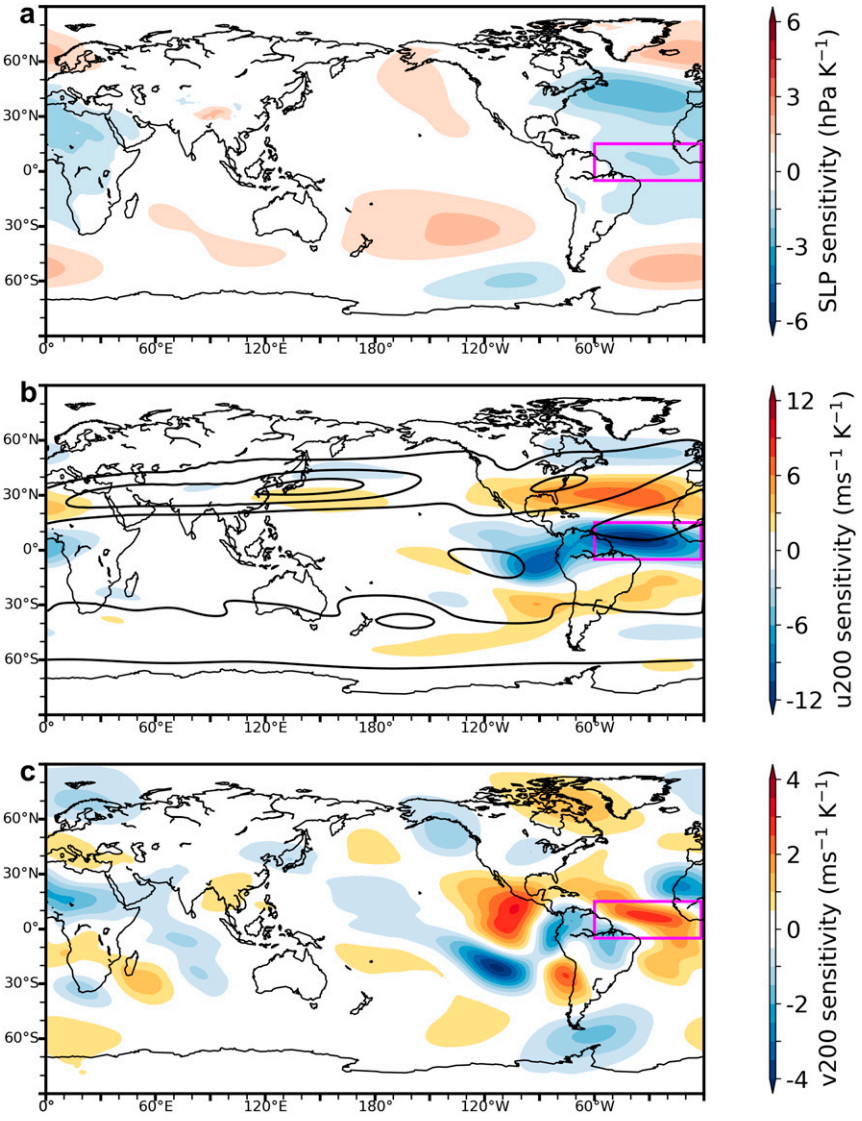

FIG. 7. Regression of the circulation responses onto SST perturbation averaged over the pink box for (a) SLP, (b) 200-hPa zonal wind, and (c) 200-hPa meridional wind. Contours in (b) show the model climatology winter (DJF) zonal wind at 200 hPa in 20 m s^{-1} intervals with the zero contour suppressed.

which has an anticyclonic region over Iceland, consistent with a negative NAO. The opposite sign of wave response over the North Atlantic and projection onto the EOF, at least in the Indian heating case, is consistent with Fletcher and Kushner (2011), who ascribe opposite cases of linear interference of a forced Rossby wave with the climatological stationary wave to Indian and Pacific SST forcing. This linear interference leads to a positive NAO for Indian Ocean forcing and a negative for Pacific Ocean forcing as observed in this study for Indian and Pacific forcing, respectively. We also perform the regression for the tropical Atlantic region (shown in Fig. 7), but this displays no clear Rossby wave forcing of the NAO. The circulation response to tropical Atlantic forcing will be discussed later in the context of the eddy-driven jet.

We also calculate the SLP and 200-hPa zonal wind responses to Indian and Pacific SSTs (Fig. 8). Consistent with previous studies (e.g., Hoskins and Karoly 1981), the local response to heating is a negative pressure anomaly. The heating also projects remotely onto the Aleutian low and the NAO via the Rossby wave as discussed. In the Indian Ocean case, the heating is associated with a pressure pattern over the North Atlantic that strongly resembles a positive NAO, while the Pacific pattern resembles the NAO to a lesser extent. The

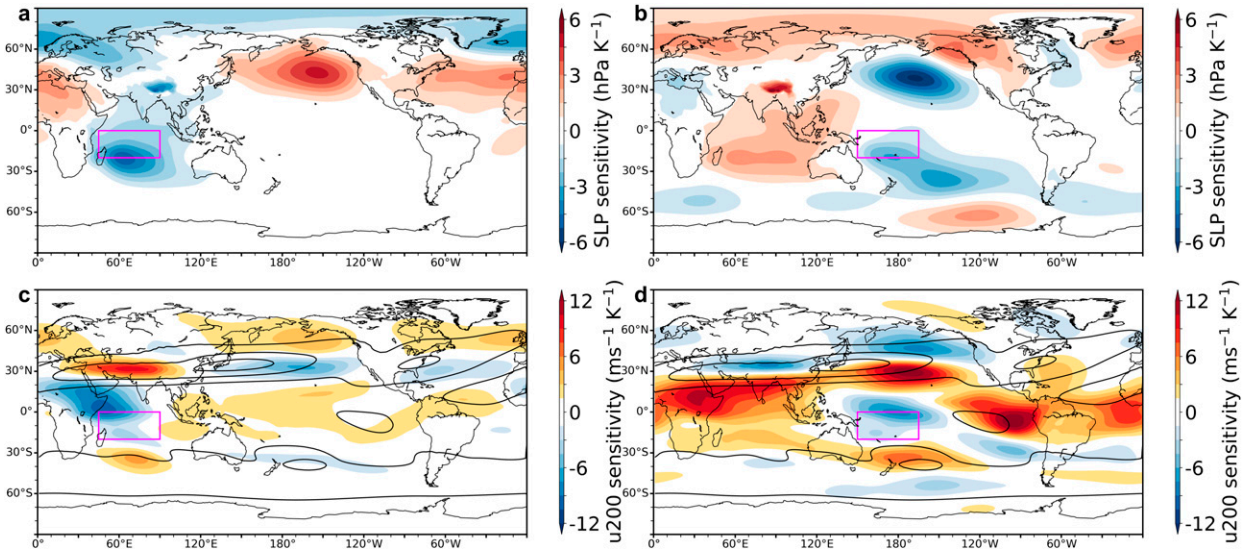

FIG. 8. Regression of the SLP responses onto the SST perturbations averaged over the pink box computed for the (a) Indian Ocean SST box and (b) Pacific Ocean SST box. Regression of the 200-hPa zonal wind responses onto the SST perturbations averaged over the pink box computed for the (c) Indian Ocean SST box and (d) Pacific Ocean SST box. Contours show the model climatology winter (DJF) zonal wind at 200 hPa in 20 m s^{-1} intervals with the zero contour suppressed.

effect on the Aleutian low is to create a ridge in the case of Indian Ocean heating and a trough in the case of Pacific Ocean heating. This is in agreement with Drouard et al. (2013) who find a Pacific ridge can act as a precursor to a positive NAO, and a trough can act as a precursor to a negative NAO. The effect of the Pacific circulation state on the NAO is also demonstrated by Franzke et al. (2004), who find that an equatorward Pacific jet can lead to a positive NAO and a poleward jet can lead to a negative NAO. However, here we see the opposite: in the Indian heating case the Pacific jet shifts poleward, while in the Pacific heating case the Pacific jet shifts equatorward. This suggests that the effect on the NAO from the tropical SSTs does not manifest via the breaking wave mechanism in Franzke et al. (2004).

2) SUMMER

We now return to investigate the SNAO in greater detail, in particular the contributions of the different basins and the reason behind the time varying skill in reconstructing the SNAO. As before, we divide the globe into three ocean basins, reconstructing the SNAO using the concurrent summer SSTs from each basin in turn (shown in Fig. 9). The correlations and standard deviations are computed over the time period where the reconstruction is skillful (1925–94). This time, it is clear that the majority of the skill in the reconstruction comes from the Pacific, where the skill is nearly the same as the global reconstruction, and the standard deviation is much higher than the other two basin reconstructions. The basin lagged predictors for summer (Fig. 10) show that directly preceding monthly SSTs are important in the Pacific, allowing the SNAO to be forecast with some level of statistically significant skill (as opposed to winter where the Pacific SSTs slightly earlier in the year were important) using the global or just Pacific SSTs from April or May. Decomposing this skill further into tropical versus midlatitude components gives a 0.29 correlation between the reconstruction using tropical May SSTs and the ERA-20C SNAO versus a 0.24 correlation from using the midlatitude SSTs. This further validates our model as it exhibits real predictability, which is not an artifact of imposed SSTs and the lack of local atmosphere–ocean coupling effect discussed earlier, as a significant portion of the skill is coming from the tropical SSTs. As in winter, the Indian SSTs appear to add some skill, but we suggest this may be due to the trend in Indian Ocean SSTs being important in summer too.

Referring back to Fig. 1, we observe that there are three significant regions in the Pacific that appear to force the SNAO. We isolate each region individually and reconstruct the SNAO just using SSTs from that region. The most skillful reconstruction comes from the positive sensitivity Pacific region (30°–10°N, 100°–150°E), which has a correlation of 0.22 with the NOAA-20C SNAO over 1925–94. We now compute the summer SST standard deviation averaged over this region, and correlate them with the 31-yr moving correlation between the NOAA-20C SNAO and reconstructed time series (using the global SSTs). Figure 11 shows that the two quantities

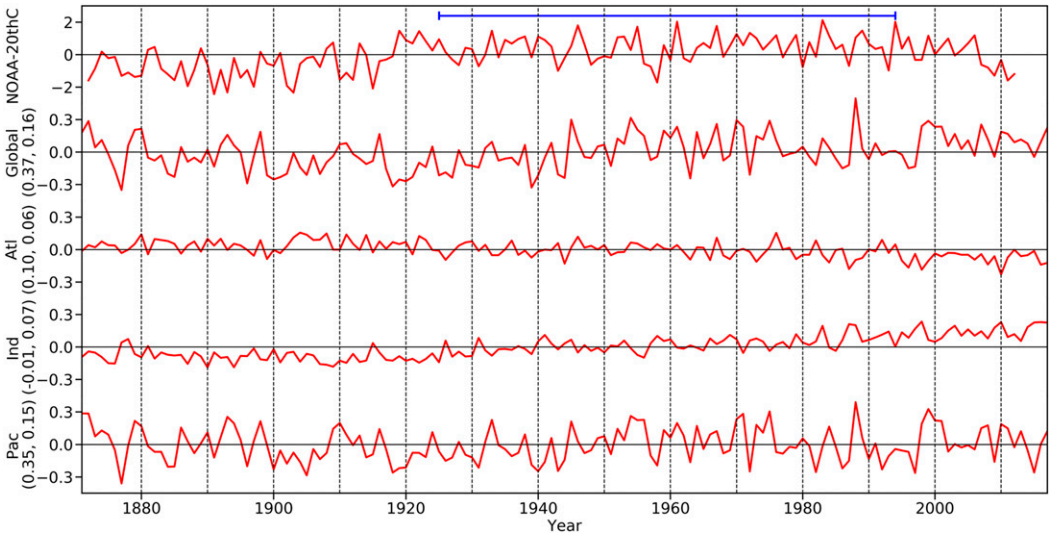

FIG. 9. NOAA-20C SNAO time series and reconstructed SNAO time series using different ocean basin summer SSTs. Global uses all SSTs, Atlantic uses 90°W–30°E, Indian uses 30°–110°E, and Pacific uses 110°E–90°W. The numbers in parentheses indicate the correlation of the time series with the NOAA-20C SNAO and the standard deviation of the time series, both computed over the period 1925–94 (shown by the blue line).

are very highly correlated (0.90), suggesting that the variability in this region is key for a skillful SNAO reconstruction. If the variability is low, then there is not a large enough signal from the SSTs to skillfully reconstruct the SNAO. An interesting facet to the SNAO reconstruction is its relation to the changing spatial pattern over the time period (see Fig. S5 and Bladé et al. 2012). In periods where the reconstruction is skillful, the positive

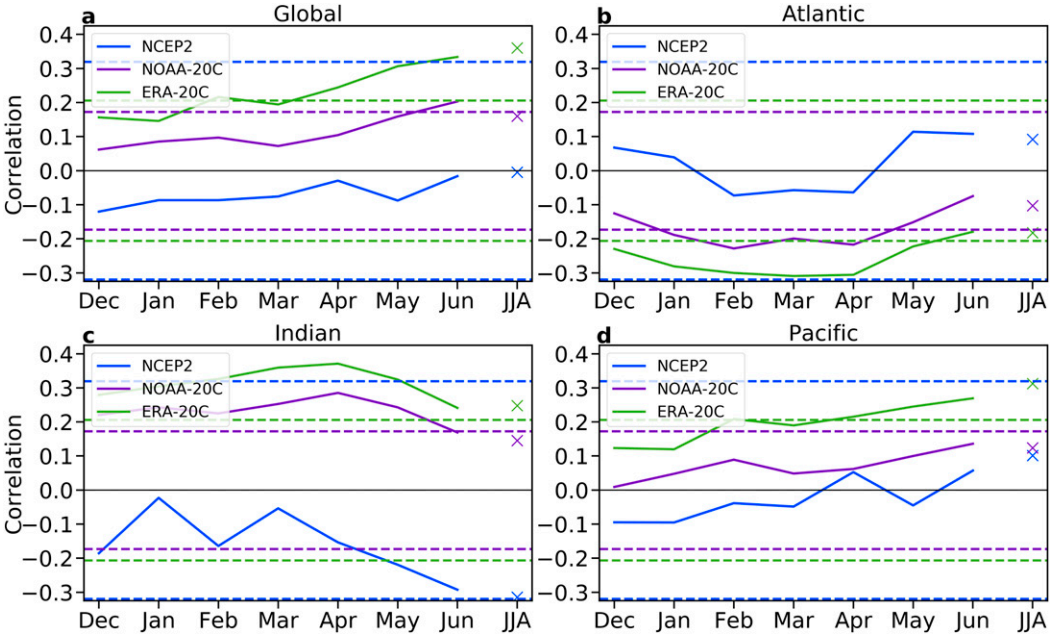

FIG. 10. Reconstructed time series correlated with reanalysis time series using SSTs (a) globally; (b) from the Atlantic basin, 90°W–30°E; (c) from the Indian basin, 30°–110°E; and (d) from the Pacific basin, 110°E–90°W. For each reanalysis, the correlation is computed using the whole period available from that reanalysis. Along the abscissa are the individual months used to reconstruct the succeeding summer (JJA) SNAO. The crosses mark the correlation of the reconstruction using the JJA SSTs with the reanalysis time series over their full time periods. The dashed lines mark the correlation required for the reconstruction and reanalysis to be correlated with a statistical significance at the 5% level, computed using a two-tailed *t* test.

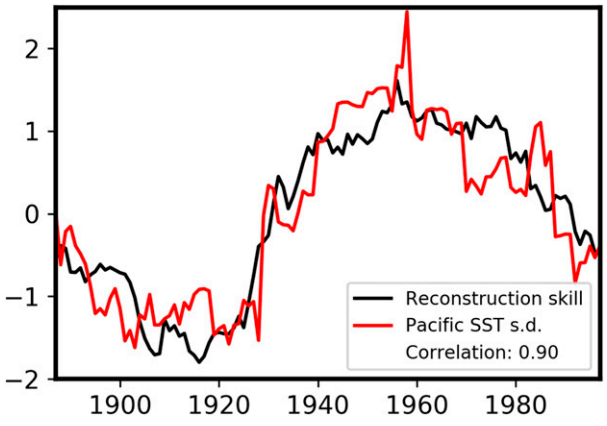

FIG. 11. Time series of the reconstruction skill, which is the standardized 31-yr moving correlation between the NOAA-20C SNAO and the reconstructed SNAO, and the standardized time series of the 31-yr moving standard deviation of the detrended SSTs in the positive sensitivity Pacific region: 30°–10°N, 100°–150°E. The year refers to the middle year of the 31-yr moving window.

center of the SNAO in observations is located further north and east over the United Kingdom, whereas in the earlier period, and to a lesser extent in the later period, the center is located over the Atlantic Ocean. Moving 51-yr EOFs from the observations (not shown) show that the positive center of action moves smoothly east and north until the 1970s, when it begins to shift back toward the Atlantic. The latitudinal and longitudinal extents of the positive center of action are both highly correlated (>0.80) with the Pacific SST standard deviation, and the SNAO reconstruction skill. Inspection of the model EOF used to compute the GTO (Fig. S3a) shows that the EOF is similar to the NOAA-20C and ERA-20C EOFs, and not the NCEP2 EOF, even though the reconstruction performs better in periods when the EOF pattern looks like the NCEP2 EOF (differences between reanalyses EOFs arise mainly due to the differing time periods covered by the reanalyses). This precludes the possibility that the reconstruction skill depends on the EOF used to compute the GTO. As an aside, we tested the statistical significance of the changing SNAO pattern by using a Monte Carlo method to construct EOFs from randomly drawn samples of 70 years from NOAA-20C. The pattern correlation coefficient between the whole time series EOF and the second half of the time series EOF fall in the bottom 0.2% of 1000 randomly constructed EOFs, demonstrating that the EOF pattern is indeed statistically significantly different in the later time period. This changing nature of the SNAO could be evidence that the SNAO, like the winter NAO, is in fact a continuum of patterns (Johnson et al. 2008).

To investigate the mechanism by which the positive sensitivity Pacific region forces the SNAO, we regress the circulation onto the SSTs in the region. Figure 12a shows the control ensemble members SLP regressed onto the set of control ensemble member principal components associated with the first EOF of SLP in summer in HadAM3P (defined over the region 20°–80°N, 90°W–40°E). Figure 12b is the 200-hPa meridional wind at each grid point across the control ensemble

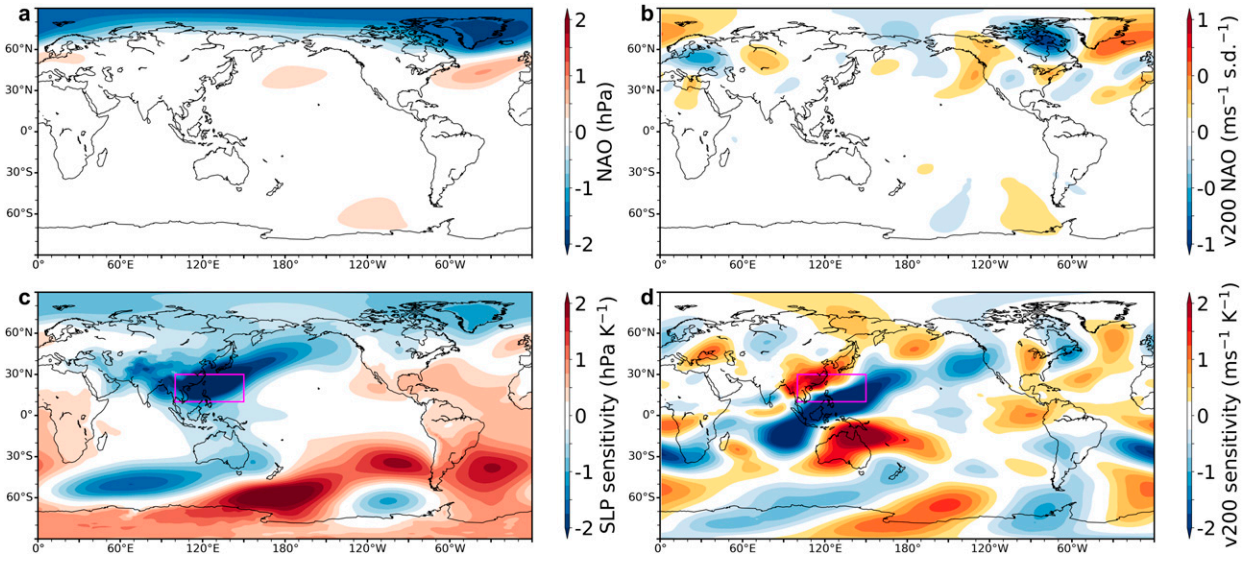

FIG. 12. (a) Control ensemble member summer SLP regressed onto principal components associated with the first EOF of summer SLP in HadAM3P (defined over the region 20°–80°N, 90°W–40°E). (b) The 200-hPa meridional wind from the HadAM3P control ensemble members regressed onto the ensemble member principal components of the first EOF. Regression of (c) SLP and (d) 200-hPa meridional wind responses onto the SST perturbations averaged over the pink box.

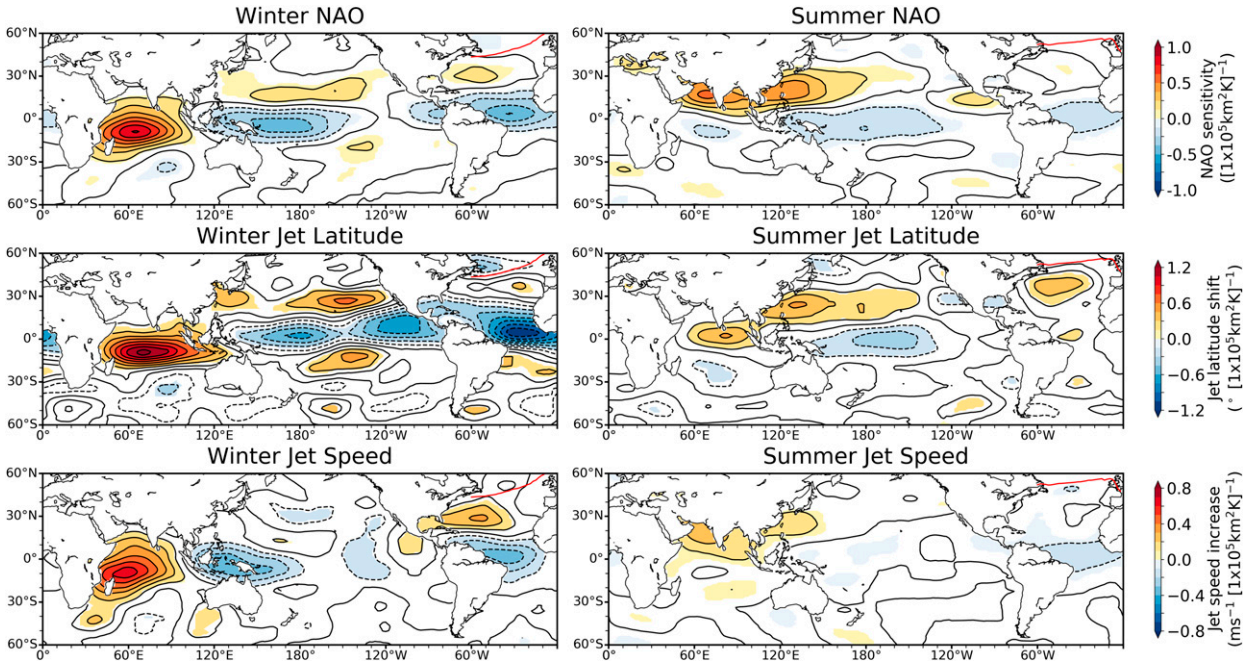

FIG. 13. Sensitivity of the North Atlantic NAO and jet indices to SST anomalies given by the $G(x')$ in Eq. (1). The top panels are reproduced from Fig. 1 for ease of comparison. A positive jet latitude shift is poleward. Shaded regions indicate statistical significance at the 5% level using a two-tailed t test. The red line indicates the position of the climatological North Atlantic storm track (taken as the maximum of the meridional component of the eddy heat flux).

members regressed onto the set of control ensemble member principal components of the model EOF. As in winter, there is a circumglobal wave pattern associated with the SNAO, with a cyclonic region over Greenland, as expected for a positive SNAO. However, the model wave train does not match the equivalent pattern computed from regressing the observed meridional wind onto the observed SNAO (Fig. S4). Figure 12c shows the SLP response to SSTs over the Pacific region. Interestingly, the pressure response over the North Atlantic looks like the SNAO in the 1940–79 period in the reanalysis (Fig. S5c), rather than the model SNAO. The 200-hPa meridional wind response (Fig. 12d) does not appear to project onto the model meridional wind associated with the first EOF, but instead contains a wave with an anticyclonic center just west of the British Isles, which is associated with the 1940–79 SNAO pattern. This provides further explanation as to why the link between the SST variability in this Pacific region and the SNAO reconstruction skill in the 1940–79 period is high. Also, the meridional wind response in Fig. 12d has a wave over North America and the North Atlantic that does resemble the wave pattern obtained from the regression of the observed meridional wind onto the observed SNAO (Fig. S4), suggesting that this mechanism does occur in the real world. Regressions of the circulation onto other high sensitivity regions in the Indian and Pacific basins (not shown) also show the SNAO response in the model arising through a cyclone/anticyclone in the same region (i.e., not projecting onto the meridional wind associated with the model EOF). This suggests that the SST forcings in the model are not proficient at forcing the model's own EOF, but can force a SNAO response that resembles that in the observed 1940–79 period, explaining the skill in this period.

b. *The eddy-driven jet*

We now focus on the North Atlantic eddy-driven jet, and compare results to the NAO findings. The GTOs for jet latitude and speed are shown in Fig. 13. The sensitivities bear resemblance to those for the NAO, and the winter jet latitude plot exhibits more widespread areas of significant sensitivity than the winter NAO. All four GTOs indicate a large degree of sensitivity to Indian Ocean SSTs. In winter, the North Atlantic tripole pattern is also clear for the jet latitude, but the jet speed only appears sensitive to the two southerly parts of the tripole. In summer, the jet latitude displays a larger sensitivity to extratropical Atlantic SSTs than the SNAO. Although the SNAO mainly represents a shift in the jet latitude (with the correlation between the NOAA-20C SNAO and jet latitude being 0.76), it is apparent that the SNAO also describes changes in jet speed too (the equivalent correlation is 0.48—similar

correlations occur for the model SNAO and jet indices). This explains why the sensitivity of the SNAO to the extratropical Atlantic SSTs does not mimic the jet latitude sensitivities, as the jet speed sensitivities also need to be considered.

The sensitivities for the jet latitude in the Atlantic and Pacific agree with the sensitivities found by Baker et al. (2017) for diabatic heating in a dry idealized model. Although the comparison between diabatic heating and SST heating is not exactly analogous, we note that the sensitivities to diabatic heating in the atmosphere found in Baker et al. (2017) are largely barotropic in nature, thus enabling useful comparison between the results found here and those in Baker et al. (2017). Heating on the equator in winter leads to an equatorward jet shift, while heating in the subtropics up to the southern flank of the jet shifts the jet poleward. This is reminiscent of the result in Lu et al. (2008): the typical El Niño response due to narrow SST increases confined to the equator is an equatorward jet shift, as opposed to the anticipated poleward shift under global warming due to broader heating extending out of the tropics. Poleward of the jet, heating acts to shift the jet equatorward (although this is not significant in the summer case). In agreement with Baker et al. (2017), there is also a cross-hemispheric sensitivity observed in the Pacific and Atlantic, with heating around 20°S forcing a poleward shift of the eddy-driven jet. The mechanism for this shift, discussed in Baker et al. (2018), could be mediated via Hadley cell changes. We leave an investigation of the mechanisms in HadAM3P for future work, but note that the circulation response to Atlantic heating (tropical Atlantic heating case shown in Fig. 7) is not inconsistent with the mechanism for jet shifts discussed in Baker et al. (2017), which manifests via changes in the low-level meridional temperature gradient. The response to tropical Atlantic heating is similar to the jet response due to narrow tropical warming (the El Niño–like response) (Lu et al. 2008), suggesting it may manifest via the mechanisms discussed in Tandon et al. (2013). The mechanism by which the Indian Ocean forces the North Atlantic circulation is via the propagation of Rossby waves (as discussed earlier), and therefore the sensitivities in this region differ to the other two ocean basins. The speed sensitivities, however, do not agree with Baker et al. (2017), who find that tropical heating up to the latitude of the storm track strengthens the jet, whereas here, SST increases in the tropics act to weaken the jet. One possible reason for this difference could be due to the regional structures in HadAM3P that are not present in the idealized model used in Baker et al. (2017), for example, differences in the subtropical and eddy-driven jet interactions. We leave an investigation into these differences for future work.

TABLE 1. Table of reconstructed jet latitude and speed skill as given by the correlation between the reconstructed time series and the reanalysis time series. Coefficients in bold are statistically significant at the 5% level using a two-tailed t test.

		NCEP2	NOAA-20C	ERA-20C
Winter	Latitude	0.26	**0.34**	**0.33**
	Speed	0.23	**0.32**	**0.34**
Summer	Latitude	0.06	**0.18**	0.14
	Speed	0.22	**0.18**	**0.24**

We reconstruct time series of the jet latitude and speed indices and compare them to the reanalysis time series. The correlation coefficients between the reconstructions and the different reanalyses are shown in Table 1 (differences in correlation predominantly arise due to the differing time periods covered by the reanalyses). In winter, the speed and latitude reconstructions are significantly correlated with the NOAA-20C and ERA-20C time series; however, the correlation drops in the later period, indicating some element of nonstationarity in the teleconnection between the SSTs and the jet speed and latitude that is not present in the NAO. As before, the GTO reconstruction performs better than the set of hindcast experiments used in Weisheimer et al. (2017) for both winter jet speed and latitude (Parker et al. 2019). For summer, the correlation coefficients are lower, in keeping with the smaller sensitivities of the two indices in the GTOs compared to winter. The highest skill in summer again occurs during the 1925–94 period for both the speed and latitude (not shown), with the latitude reconstruction skill dropping off in the later period, but the speed reconstruction skill not.

The skill in reconstructing the NAO over the longer reanalysis periods is greater than for the individual jet indices, suggesting that the skill in the NAO may be coming from both jet latitude and speed. Following Parker et al. (2019), we perform a multiple linear regression to determine the relationship between the NAO and the jet latitude and speed in the reconstruction, with the aim of attributing the predictable NAO signal to jet latitude, speed, or both. In winter, the regression coefficients for the reconstruction are 0.60 for jet speed and 0.56 for jet latitude, combining to explain 67% of the NAO variability over the reconstruction time period. In summer, the regression coefficients for the reconstruction are 0.28 for jet speed and 0.78 for jet latitude, combining to explain 69% of the NAO variability. The coefficients for NOAA-20C are 0.32 and 0.81 for winter jet speed and latitude, respectively (explaining 76% of the variability), and 0.34 and 0.69 for

TABLE 2. Table of changing NAO skill for various terms in the NAO multilinear regression. The slow and fast columns show the correlation between the NOAA-20C and reconstructed time series when that element of the reconstructed NAO calculation is omitted. The correlation without omitting any elements is 0.43 in winter and 0.21 in summer.

		Slow	Fast
Winter	Latitude	0.39	0.28
	Speed	0.46	0.42
Summer	Latitude	0.25	0.15
	Speed	0.20	0.16

summer jet speed and latitude (explaining 59% of the variability). While the summer coefficients are fairly similar between the reconstruction and the reanalysis, it seems the winter NAO in the model is over dependent on the jet speed. This could be due to the winter jet being too zonal and too strong in the model (see mean jet biases in Fig. S1). The jet also has a higher ratio of jet speed standard deviation to the jet latitude standard deviation (0.46 in the model vs 0.37 in NOAA-20C) suggesting that the model has a greater component of pulsing variability than shifting variability compared to the reanalysis, consistent with the jet being further poleward in the model climatology than in NOAA-20C (48.2° vs 47.2° in winter). This is consistent with Barnes and Hartmann (2011) who observe that the leading mode of zonal-wind variability transitions from a shift to a pulse as the eddy-driven jet moves poleward. In summer, there is no difference between the standard deviations ratios, even though the model jet is further poleward (50.6° vs 48.8°).

To ascertain the time scales on which the jet features are providing skill to the NAO, we perform a multiple linear regression following Parker et al. (2019). We use the jet latitude and speed on both fast and slow time scales as predictors for the NAO. We then remove each feature in turn to determine their contribution to the NAO skill. The slow components are computed using an 11-yr low-pass Lanczos filter with 11 weights (Duchon 1979), and the fast components using an 11-yr high-pass Lanczos filter. Table 2 shows the correlations obtained between the NOAA-20C time series and regression constructed time series as each component is individually removed. In winter, it is only the removal of the fast component of the latitude that appreciably reduces the skill (the same is true for 31-yr filter windows, not shown). This agrees with Woollings et al. (2014) in the sense that on fast time scales the NAO is dominated by variations in jet latitude, however, the relationship they find on longer time scales between the jet speed and NAO is not captured in this method. In summer, both the fast time scale speed and latitude appear to be important, and the removal of the slow time scale latitude actually slightly increases the reconstruction skill. From this simple linear approach it appears that it is the faster time scales that give predictability to the NAO, suggesting again that the decadal Indian Ocean influence may be less important than previous studies have suggested.

c. *Limitations*

The results discussed above are from prescribed SST experiments and are derived under a linear assumption. This means that there are several limitations of the study, which we now proceed to discuss. Clearly when prescribing SSTs, the ocean is unable to respond to atmospheric processes, and so the first issue is related to the lack of atmosphere–ocean coupling. Barsugli and Battisti (1998) investigate the effect of coupling on midlatitude variability, finding that it is important in the midlatitudes for correctly simulating the low-frequency atmospheric thermal variance. Bretherton and Battisti (2000) extend the analysis further, showing that the useful predictability associated with midlatitude SST anomalies may be limited to around 6 months. The problem lies in the fact that the observed midlatitude SSTs have some component forced from the atmosphere, and so by imposing observed SSTs in a model, some information about the correct atmospheric state is already being prescribed.

The mechanism acting in the Barsugli and Battisti (1998) model is reduced thermal damping, which acts as a positive feedback giving a positive correlation between the atmosphere and the local SSTs. Our analysis shows that the NAO is sensitive to remote SSTs, often in the tropics, and this mechanism does not apply to remote linkages. If we reconstruct the NAO using only SSTs southward of 30°N, we obtain a reconstruction that has a correlation coefficient with the NOAA-20C NAO of 0.36, compared to 0.30 correlation when using SSTs north of 30°N. This suggests that there is a significant element of predictability arising from the tropical SSTs, which is not impacted by the lack of atmosphere–ocean coupling in the model. The coupling effect is also more important on longer time scales (Bretherton and Battisti 2000), whereas the skill in our reconstructions comes from higher-frequency, interannual SST forcing. We also observe skill in using preceding SSTs to forecast the NAO in both winter and summer, where this lack of coupling is not an issue (and as discussed earlier, the skill comes from the tropics).

There is also an issue specific to atmosphere–ocean interactions in the Indian Ocean. Annamalai et al. (2007) find that parts of the Indian Ocean, responding to

atmospheric forcing, warm during El Niño. This is supported by Klein et al. (1999), who show that during ENSO events, cloud cover is reduced over the Indian Ocean, allowing more solar radiation to warm the SSTs. Furthermore, Copsey et al. (2006) show that the warming trend in Indian Ocean SSTs during 1950–96 is associated with increases in SLP, which is at odds with prescribed SST experiments that show decreases in SLP due to increased SSTs. It appears then that positive SST anomalies over the Indian Ocean can arise as a result of atmospheric descent, high pressure, clear skies, and increased downward shortwave radiation. On top of this, the dominant modes of SST variability in the Indian Ocean are associated with an ENSO signal in the Pacific (Fig. S6). This suggests that in the real world, much of the SST variability in the Indian Ocean is being forced by ENSO, via the atmosphere, rather than the SSTs forcing the atmosphere. This does not preclude the Indian Ocean teleconnection that we find in the model occurring in the real world, but has implications when using Indian Ocean SSTs combined with the GTO to reconstruct the NAO. This is because much of the SST variability is being forced by the atmosphere and in these periods the SSTs may then not be forcing the atmosphere, rendering the teleconnection inactive. This would lead to spurious signals when using the GTO combined with Indian Ocean SSTs to reconstruct the NAO.

The matter is further complicated by limitations in the linearity of the atmospheric response to combined forcing from the Indian and Pacific basins. Fletcher and Kushner (2011) show that the atmospheric circulation response to combined Indian and Pacific SST forcing over the Indian Ocean Basin is different from the sum of the responses to the individual basin forcings. This shows that the linearity assumption of the atmospheric response to SSTs breaks down over the Indian Ocean. This nonlinearity seems to arise from the fact that the circulation response to SSTs in both basins interferes with a climatological stationary wave in an opposing manner (Annamalai et al. 2007; Fletcher and Kushner 2011). As a large part of Indian Ocean SST variability appears to coincide with variations in the Pacific Ocean SSTs (Fig. S6), this suggests that when Indian Ocean SSTs are anomalously warm and would be expected to drive a positive NAO signal given the GTO, the Pacific SSTs would also be anomalously warm, thus destructively interfering with the Indian Ocean teleconnection. This would cause errors to occur in the reconstruction of the NAO from the linear reconstructed using the GTO when the Indian Ocean SST anomalies (combined with Pacific Ocean SST anomalies) are large. As mentioned earlier, these effects do not preclude the Indian Ocean to NAO teleconnection occurring in the real world. In fact, Fletcher and Cassou (2015) show using a coupled model that the Indian Ocean can force the NAO, once isolated from ENSO variability. Further work is clearly needed to investigate the complex interactions between ENSO, tropical SSTs and teleconnections that force the NAO to confirm if these interactions are indeed the reason why we do not observe any skill in reconstructing the NAO from the Indian Ocean SSTs. In any case, the sensitivity of the NAO to the Indian Ocean SSTs should be treated with caution.

Another potential limitation arises due to the relatively low vertical resolution of the model in the stratosphere. This could preclude teleconnections present in the real world that propagate via stratospheric pathways, which are better simulated with models with higher vertical resolution in the stratosphere (Hardiman et al. 2012). This might result in teleconnections observed in modeling studies between the tropical Pacific and extratropical North Atlantic in winter (e.g., Bell et al. 2009; Ineson and Scaife 2009) not occurring fully in the HadAM3P model. If this were the case, it would mean that the sensitivities of the NAO and jet to tropical Pacific SSTs are underestimated, and may mean in reality that the Pacific Ocean is a stronger driver of the winter NAO than the results in Figs. 4 and 5 show. Further to this, some teleconnections forced by tropical SSTs have been shown to act via independent tropospheric and stratospheric pathways, which affect the extratropical circulation and temperature differently (Butler et al. 2014). By potentially not capturing these stratospheric pathways, it is possible that this study overestimates the importance of the tropospheric pathways. Further work using a model with a high-resolution stratosphere is clearly necessary to confirm if this is the case.

The quality of the SST dataset could also have an impact on our results. The quality of the historical SST product in the early period is poorer than in the later period (due to fewer observations and the need to use statistical methods to infill the gaps in the data). This can be seen by comparing SST products and noting the increase in variability between them in early historical periods (Yasunaka and Hanawa 2011; Hirahara et al. 2014), and by comparing the SST products to independent observations (Huang et al. 2018). The time varying quality of the SST dataset could affect the apparent time varying skill of the reconstruction method. In winter, this seems not to be a problem, given the fairly constant level of reconstruction skill. In summer however, the poor SNAO reconstruction skill before 1925 could be in part due to the paucity of the SST data, although this would not impact the poor reconstruction skill in the period from 1995 onward. Clearly there are

limitations of working with the long SST dataset that need to be considered when interpreting the results.

4. Conclusions

This study used a linear statistical–dynamic method applied to a large ensemble of randomly perturbed SSTs to investigate the North Atlantic circulation sensitivity to SSTs. We verified the winter NAO sensitivities found in Li and Forest (2014) and additionally showed the regions where the SNAO is sensitive to changes in SSTs, identifying several key regions. The Atlantic tripole pattern is present in both winter and summer sensitivity maps, in particular the tropical Atlantic node of the tripole. Over the Indian Ocean there is a large SST monopole in winter and dipole in summer that the NAO is sensitive to, while in the west Pacific there is a dipole in both seasons. Using the GTO, we demonstrated skill in reconstructing both the winter NAO and SNAO, although there is some nonstationarity in the skill in reconstructing the SNAO that appears to arise from the Pacific SST variability. In winter, the reconstruction performs better than a recent ensemble of atmosphere-only hindcast experiments and the reconstruction skill does not display the same drop-off in skill in the 1950–70s as in the hindcasts (Weisheimer et al. 2017).

When using concurrent SSTs to reconstruct the NAO, the Atlantic SSTs, and to a lesser extent the Pacific SSTs, are important in providing the skill in the reconstruction. We demonstrated a novel application of the linear reconstruction method to make forecasts of the NAO and SNAO. Using SSTs before the winter season, we were able to make a skillful winter NAO forecast. In summer, we showed that the Pacific SSTs are the most important in providing skill, and we demonstrated using this method that skillful SNAO forecasts can be made, which to this date have not been reported elsewhere (Dunstone et al. 2018). When forecasting the NAO in both winter and summer, the tropics appear relatively more important than when reconstructing the NAO using the concurrent SSTs. We also find evidence for nonstationarity in the SNAO, and the tropical teleconnections that appear to force it, which we suggest arises due to decadal SST variability in the west Pacific.

For the first time, we also used the linear method to identify the North Atlantic eddy-driven jet latitude and speed sensitivities to SSTs. They display broadly similar patterns to the NAO, although some differences do exist between all three sensitivity maps. We demonstrated similar levels of skill in reconstructing time series of the jet latitude and speed, showing that in winter, the speed and latitude contribute roughly equally to the variability in the NAO reconstruction, whereas in summer the latitude contributes most of the variability in the reconstruction. Investigating the importance of fast and slow varying time scales in the jet latitude and speed, it seems that the fast time scale jet latitude is important for reconstructing the winter NAO, while both fast jet latitude and speed are important for reconstructing the SNAO.

The sensitivities we observe for the NAO and jet are in broad agreement with previous literature, identifying the Indian Ocean region (as seen in, e.g., Hoerling et al. 2001, 2004; Bader and Latif 2003, 2005; Fletcher and Kushner 2011) and Atlantic tripole (as seen in, e.g., Rodwell et al. 1999; Czaja and Frankignoul 2002; Peng et al. 2002; Wang et al. 2004) as important sensitivity regions. In agreement with Fletcher and Kushner (2011), the Indian Ocean sensitivity appears to arise from, in winter at least, the forcing of Rossby waves that constructively interfere with the climatological stationary wave, thus forcing a positive NAO response. To a lesser extent, the Pacific Ocean SSTs produce a Rossby wave that destructively interferes with the climatological wave, thus forcing a negative NAO. The jet latitude sensitivities in the Pacific and Atlantic basins agree with idealized sensitivity studies (Lu et al. 2008; Baker et al. 2017), and contain the equatorward jet shift seen for El Niño–like forcing and the poleward shift for broader tropical heating as in the global warming case.

Here we have only considered the impact of tropical and midlatitude SSTs on the NAO and jet, when there are numerous other potentially important drivers such as sea ice (e.g., Pedersen et al. 2016), snow (e.g., Henderson et al. 2018), the sun (e.g., Gray et al. 2016), the stratosphere (e.g., Scaife et al. 2005), and atmosphere–ocean coupling effects (e.g., Czaja et al. 2013). Therefore, the fact that we see some predictive skill in both winter and summer in reconstructing the NAO using a purely linear method demonstrates that SSTs are an important driver of North Atlantic atmospheric circulation. There may also be other nonlinear SST effects that the RPM does not capture, and these effects are not quantified in this current study. Given the importance of the NAO and jet on European, North American, and North African weather and climate (e.g., Visbeck et al. 2001; Hurrell and Deser 2009; Cattiaux et al. 2010; Bladé et al. 2012; Schaller et al. 2016), it is vitally important that we can forecast the NAO skillfully. The ability of the RPM to skillfully reconstruct the NAO from SSTs therefore provides a highly useful tool for forecasting, also providing direct attribution of where the signals are coming from in the system.

Acknowledgments. This work was supported by the Natural Environment Research Council (Grant NE/L002612/1 and NERC SummerTIME project, Grant NE/M005887/1). We thank the three anonymous reviewers

for their comments that helped to improve the manuscript. We thank our colleagues at the Oxford eResearch Centre: A. Bowery, S. Sparrow, S. Li, and D. Wallom for their technical expertise. We thank the Met Office Hadley Centre PRECIS team for their technical and scientific support for the development and application of weather@home. Finally, we thank all of the volunteers who have donated their computing time to climateprediction.net and weather@home.

REFERENCES

Allen, M., 1999: Do-it-yourself climate prediction. *Nature*, **401**, 642–642, https://doi.org/10.1038/44266.

Annamalai, H., H. Okajima, and M. Watanabe, 2007: Possible impact of the Indian Ocean SST on the Northern Hemisphere circulation during El Niño. *J. Climate*, **20**, 3164–3189, https://doi.org/10.1175/JCLI4156.1.

Bader, J., and M. Latif, 2003: The impact of decadal-scale Indian Ocean sea surface temperature anomalies on Sahelian rainfall and the North Atlantic Oscillation. *Geophys. Res. Lett.*, **30**, 2169, https://doi.org/10.1029/2003GL018426.

——, and ——, 2005: North Atlantic Oscillation response to anomalous Indian Ocean SST in a coupled GCM. *J. Climate*, **18**, 5382–5389, https://doi.org/10.1175/JCLI3577.1.

Baker, H. S., T. Woollings, and C. Mbengue, 2017: Eddy-driven jet sensitivity to diabatic heating in an idealized GCM. *J. Climate*, **30**, 6413–6431, https://doi.org/10.1175/JCLI-D-16-0864.1.

——, C. Mbengue, and T. Woollings, 2018: Seasonal sensitivity of the Hadley cell and cross-hemispheric responses to diabatic heating in an idealized GCM. *Geophys. Res. Lett.*, **45**, 2533–2541, https://doi.org/10.1002/2018GL077013.

Barnes, E. A., and D. L. Hartmann, 2011: Rossby wave scales, propagation, and the variability of eddy-driven jets. *J. Atmos. Sci.*, **68**, 2893–2908, https://doi.org/10.1175/JAS-D-11-039.1.

Barsugli, J. J., and D. S. Battisti, 1998: The basic effects of atmosphere–ocean thermal coupling on midlatitude variability. *J. Atmos. Sci.*, **55**, 477–493, https://doi.org/10.1175/1520-0469(1998)055<0477:TBEOAO>2.0.CO;2.

——, and P. D. Sardeshmukh, 2002: Global atmospheric sensitivity to tropical SST anomalies throughout the Indo-Pacific basin. *J. Climate*, **15**, 3427–3442, https://doi.org/10.1175/1520-0442(2002)015<3427:GASTTS>2.0.CO;2.

——, S.-I. Shin, and P. D. Sardeshmukh, 2006: Sensitivity of global warming to the pattern of tropical ocean warming. *Climate Dyn.*, **27**, 483–492, https://doi.org/10.1007/s00382-006-0143-7.

Bell, C. J., L. J. Gray, A. J. Charlton-Perez, M. M. Joshi, and A. A. Scaife, 2009: Stratospheric communication of El Niño teleconnections to European winter. *J. Climate*, **22**, 4083–4096, https://doi.org/10.1175/2009JCLI2717.1.

Bladé, I., B. Liebmann, D. Fortuny, and G. J. van Oldenborgh, 2012: Observed and simulated impacts of the summer NAO in Europe: Implications for projected drying in the Mediterranean region. *Climate Dyn.*, **39**, 709–727, https://doi.org/10.1007/s00382-011-1195-x.

Bretherton, C. S., and D. S. Battisti, 2000: An interpretation of the results from atmospheric general circulation models forced by the time history of the observed sea surface temperature distribution. *Geophys. Res. Lett.*, **27**, 767–770, https://doi.org/10.1029/1999GL010910.

Butler, A. H., L. M. Polvani, and C. Deser, 2014: Separating the stratospheric and tropospheric pathways of El Niño–Southern Oscillation teleconnections. *Environ. Res. Lett.*, **9**, 024014, https://doi.org/10.1088/1748-9326/9/2/024014.

Cassou, C., C. Deser, and M. A. Alexander, 2007: Investigating the impact of reemerging sea surface temperature anomalies on the winter atmospheric circulation over the North Atlantic. *J. Climate*, **20**, 3510–3526, https://doi.org/10.1175/JCLI4202.1.

Cattiaux, J., R. Vautard, C. Cassou, P. Yiou, V. Masson-Delmotte, and F. Codron, 2010: Winter 2010 in Europe: A cold extreme in a warming climate. *Geophys. Res. Lett.*, **37**, L20704, https://doi.org/10.1029/2010GL044613.

Colfescu, I., E. K. Schneider, and H. Chen, 2013: Consistency of 20th century sea level pressure trends as simulated by a coupled and uncoupled GCM. *Geophys. Res. Lett.*, **40**, 3276–3280, https://doi.org/10.1002/grl.50545.

Compo, G. P., and Coauthors, 2011: The Twentieth Century Reanalysis Project. *Quart. J. Roy. Meteor. Soc.*, **137**, 1–28, https://doi.org/10.1002/qj.776.

Copsey, D., R. Sutton, and J. R. Knight, 2006: Recent trends in sea level pressure in the Indian Ocean region. *Geophys. Res. Lett.*, **33**, L19712, https://doi.org/10.1029/2006GL027175.

Czaja, A., and C. Frankignoul, 2002: Observed impact of Atlantic SST anomalies on the North Atlantic Oscillation. *J. Climate*, **15**, 606–623, https://doi.org/10.1175/1520-0442(2002)015<0606:OIOASA>2.0.CO;2.

——, A. W. Robertson, and T. Huck, 2013: The role of Atlantic Ocean–atmosphere coupling in affecting North Atlantic Oscillation variability. *The North Atlantic Oscillation: Climatic Significance and Environmental Impact*, *Geophys. Monogr.*, Vol. 134, Amer. Geophys. Union, 147–172, https://doi.org/10.1029/134GM07.

Drouard, M., G. Rivière, and P. Arbogast, 2013: The North Atlantic Oscillation response to large-scale atmospheric anomalies in the northeastern Pacific. *J. Atmos. Sci.*, **70**, 2854–2874, https://doi.org/10.1175/JAS-D-12-0351.1.

Duchon, C. E., 1979: Lanczos filtering in one and two dimensions. *J. Appl. Meteor.*, **18**, 1016–1022, https://doi.org/10.1175/1520-0450(1979)018<1016:LFIOAT>2.0.CO;2.

Dunstone, N., D. Smith, A. Scaife, L. Hermanson, R. Eade, N. Robinson, M. Andrews, and J. Knight, 2016: Skilful predictions of the winter North Atlantic Oscillation one year ahead. *Nat. Geosci.*, **9**, 809–814, https://doi.org/10.1038/ngeo2824.

——, and Coauthors, 2018: Skilful seasonal predictions of summer European rainfall. *Geophys. Res. Lett.*, **45**, 3246–3254, https://doi.org/10.1002/2017GL076337.

Fletcher, C. G., and P. J. Kushner, 2011: The role of linear interference in the annular mode response to tropical SST forcing. *J. Climate*, **24**, 778–794, https://doi.org/10.1175/2010JCLI3735.1.

——, and C. Cassou, 2015: The dynamical influence of separate teleconnections from the Pacific and Indian Oceans on the northern annular mode. *J. Climate*, **28**, 7985–8002, https://doi.org/10.1175/JCLI-D-14-00839.1.

Folland, C. K., J. Knight, H. W. Linderholm, D. Fereday, S. Ineson, and J. W. Hurrell, 2009: The summer North Atlantic Oscillation: Past, present, and future. *J. Climate*, **22**, 1082–1103, https://doi.org/10.1175/2008JCLI2459.1.

Franzke, C., S. Lee, and S. B. Feldstein, 2004: Is the North Atlantic Oscillation a breaking wave? *J. Atmos. Sci.*, **61**, 145–160, https://doi.org/10.1175/1520-0469(2004)061<0145:ITNAOA>2.0.CO;2.

Gordon, C., C. Cooper, C. A. Senior, H. Banks, J. M. Gregory, T. C. Johns, J. F. B. Mitchell, and R. A. Wood, 2000: The simulation

of SST, sea ice extents and ocean heat transports in a version of the Hadley Centre coupled model without flux adjustments. *Climate Dyn.*, **16**, 147–168, https://doi.org/10.1007/s003820050010.

Gray, L. J., T. J. Woollings, M. Andrews, and J. Knight, 2016: Eleven-year solar cycle signal in the NAO and Atlantic/European blocking. *Quart. J. Roy. Meteor. Soc.*, **142**, 1890–1903, https://doi.org/10.1002/qj.2782.

Guillod, B. P., and Coauthors, 2017: weather@home 2: Validation of an improved global–regional climate modelling system. *Geosci. Model Dev.*, **10**, 1849–1872, https://doi.org/10.5194/gmd-10-1849-2017.

Hardiman, S. C., N. Butchart, T. J. Hinton, S. M. Osprey, and L. J. Gray, 2012: The effect of a well-resolved stratosphere on surface climate: Differences between CMIP5 simulations with high and low top versions of the Met Office climate model. *J. Climate*, **25**, 7083–7099, https://doi.org/10.1175/JCLI-D-11-00579.1.

Henderson, G. R., Y. Peings, J. C. Furtado, and P. J. Kushner, 2018: Snow–atmosphere coupling in the Northern Hemisphere. *Nat. Climate Change*, **8**, 954–963, https://doi.org/10.1038/s41558-018-0295-6.

Hirahara, S., M. Ishii, and Y. Fukuda, 2014: Centennial-scale sea surface temperature analysis and its uncertainty. *J. Climate*, **27**, 57–75, https://doi.org/10.1175/JCLI-D-12-00837.1.

Hoerling, M. P., J. W. Hurrell, and T. Xu, 2001: Tropical origins for recent North Atlantic climate change. *Science*, **292**, 90–92, https://doi.org/10.1126/science.1058582.

——, ——, ——, G. T. Bates, and A. S. Phillips, 2004: Twentieth century North Atlantic climate change. Part II: Understanding the effect of Indian Ocean warming. *Climate Dyn.*, **23**, 391–405, https://doi.org/10.1007/s00382-004-0433-x.

——, and Coauthors, 2014: Northeast Colorado extreme rains interpreted in a climate change context [in "Explaining Extreme Events of 2013 from a Climate Perspective"]. *Bull. Amer. Meteor. Soc.*, **95** (9), S15–S18, https://doi.org/10.1175/1520-0477-95.9.S1.1.

Hoskins, B. J., and D. J. Karoly, 1981: The steady linear response of a spherical atmosphere to thermal and orographic forcing. *J. Atmos. Sci.*, **38**, 1179–1196, https://doi.org/10.1175/1520-0469(1981)038<1179:TSLROA>2.0.CO;2.

Huang, B., W. Angel, T. Boyer, L. Cheng, G. Chepurin, E. Freeman, C. Liu, and H.-M. Zhang, 2018: Evaluating SST analyses with independent ocean profile observations. *J. Climate*, **31**, 5015–5030, https://doi.org/10.1175/JCLI-D-17-0824.1.

Hurrell, J. W., 1995: Decadal trends in the North Atlantic Oscillation: Regional temperatures and precipitation. *Science*, **269**, 676–679, https://doi.org/10.1126/science.269.5224.676.

——, and C. Deser, 2009: North Atlantic climate variability: The role of the North Atlantic Oscillation. *J. Mar. Syst.*, **78**, 28–41, https://doi.org/10.1016/j.jmarsys.2008.11.026.

——, J. J. Hack, D. Shea, J. M. Caron, and J. Rosinski, 2008: A new sea surface temperature and sea ice boundary dataset for the community atmosphere model. *J. Climate*, **21**, 5145–5153, https://doi.org/10.1175/2008JCLI2292.1.

——, Y. Kushnir, G. Ottersen, and M. H. Visbeck, 2013: An overview of the North Atlantic Oscillation. *The North Atlantic Oscillation: Climatic Significance and Environmental Impact*, *Geophys. Monogr.*, Vol. 134, Amer. Geophys. Union, 1–35, https://doi.org/10.1002/9781118669037.fmatter.

Ineson, S., and A. A. Scaife, 2009: The role of the stratosphere in the European climate response to El Niño. *Nat. Geosci.*, **2**, 32–36, https://doi.org/10.1038/ngeo381.

Jin, F., and B. J. Hoskins, 1995: The direct response to tropical heating in a baroclinic atmosphere. *J. Atmos. Sci.*, **52**, 307–319, https://doi.org/10.1175/1520-0469(1995)052<0307:TDRTTH>2.0.CO;2.

Johnson, N. C., S. B. Feldstein, and B. Tremblay, 2008: The continuum of Northern Hemisphere teleconnection patterns and a description of the NAO shift with the use of self-organizing maps. *J. Climate*, **21**, 6354–6371, https://doi.org/10.1175/2008JCLI2380.1.

Kanamitsu, M., W. Ebisuzaki, J. Woollen, S.-K. Yang, J. J. Hnilo, M. Fiorino, and G. L. Potter, 2002: NCEP-DOE AMIP-II Reanalysis (R-2). *Bull. Amer. Meteor. Soc.*, **83**, 1631–1644, https://doi.org/10.1175/BAMS-83-11-1631.

King, M. P., F. Kucharski, and F. Molteni, 2010: The roles of external forcings and internal variabilities in the Northern Hemisphere atmospheric circulation change from the 1960s to the 1990s. *J. Climate*, **23**, 6200–6220, https://doi.org/10.1175/2010JCLI3239.1.

Klein, S. A., B. J. Soden, and N.-C. Lau, 1999: Remote sea surface temperature variations during ENSO: Evidence for a tropical atmospheric bridge. *J. Climate*, **12**, 917–932, https://doi.org/10.1175/1520-0442(1999)012<0917:RSSTVD>2.0.CO;2.

Kucharski, F., F. Molteni, and A. Bracco, 2006: Decadal interactions between the western tropical Pacific and the North Atlantic Oscillation. *Climate Dyn.*, **26**, 79–91, https://doi.org/10.1007/s00382-005-0085-5.

Kumar, A., and M. Chen, 2018: Causes of skill in seasonal predictions of the Arctic Oscillation. *Climate Dyn.*, **51**, 2397–2411, https://doi.org/10.1007/s00382-017-4019-9.

Kushnir, Y., W. A. Robinson, P. Chang, and A. W. Robertson, 2006: The physical basis for predicting Atlantic sector seasonal-to-interannual climate variability. *J. Climate*, **19**, 5949–5970, https://doi.org/10.1175/JCLI3943.1.

Li, W., and C. E. Forest, 2014: Estimating the sensitivity of the atmospheric teleconnection patterns to SST anomalies using a linear statistical method. *J. Climate*, **27**, 9065–9081, https://doi.org/10.1175/JCLI-D-14-00231.1.

——, ——, and J. Barsugli, 2012: Comparing two methods to estimate the sensitivity of regional climate simulations to tropical SST anomalies. *J. Geophys. Res.*, **117**, D20103, https://doi.org/10.1029/2011JD017186.

Lu, J., G. Chen, and D. M. W. Frierson, 2008: Response of the zonal mean atmospheric circulation to El Niño versus global warming. *J. Climate*, **21**, 5835–5851, https://doi.org/10.1175/2008JCLI2200.1.

Massey, N., and Coauthors, 2015: weather@home-development and validation of a very large ensemble modelling system for probabilistic event attribution. *Quart. J. Roy. Meteor. Soc.*, **141**, 1528–1545, https://doi.org/10.1002/qj.2455.

Mitchell, D., and Coauthors, 2017: Assessing mid-latitude dynamics in extreme event attribution systems. *Climate Dyn.*, **48**, 3889–3901, https://doi.org/10.1007/s00382-016-3308-z.

O'Reilly, C. H., T. Woollings, L. Zanna, and A. Weisheimer, 2018: The impact of tropical precipitation on summertime Euro-Atlantic circulation via a circumglobal wave train. *J. Climate*, **31**, 6481–6504, https://doi.org/10.1175/JCLI-D-17-0451.1.

Parker, T., T. Woollings, A. Weisheimer, L. Baker, C. O'Reilly, and L. Shaffrey, 2019: Seasonal predictability of the winter North Atlantic Oscillation from a jet stream perspective. *Geophys. Res. Lett.*, **46**, https://doi.org/10.1029/2019GL084402, in press.

Pedersen, R. A., I. Cvijanovic, P. L. Langen, and B. M. Vinther, 2016: The impact of regional arctic sea ice loss on atmospheric circulation and the NAO. *J. Climate*, **29**, 889–902, https://doi.org/10.1175/JCLI-D-15-0315.1.

Peng, S., W. A. Robinson, and S. Li, 2002: North Atlantic SST Forcing of the NAO and relationships with intrinsic hemispheric variability. *Geophys. Res. Lett.*, **29**, 1171–1174, https://doi.org/10.1029/2001GL014043.

Poli, P., and Coauthors, 2016: ERA-20C: An Atmospheric Reanalysis of the Twentieth Century. *J. Climate*, **29**, 4083–4097, https://doi.org/10.1175/JCLI-D-15-0556.1.

Pope, V. D., M. L. Gallani, P. R. Rowntree, and R. A. Stratton, 2000: The impact of new physical parametrizations in the Hadley Centre climate model: HadAM3. *Climate Dyn.*, **16**, 123–146, https://doi.org/10.1007/s003820050009.

Rayner, N. A., D. E. Parker, E. B. Horton, C. K. Folland, L. V. Alexander, D. P. Rowell, E. C. Kent, and A. Kaplan, 2003: Global analyses of sea surface temperature, sea ice, and night marine air temperature since the late nineteenth century. *J. Geophys. Res.*, **108**, 4407, https://doi.org/10.1029/2002JD002670.

Rodwell, M. J., D. P. Rowell, and C. K. Folland, 1999: Oceanic forcing of the wintertime North Atlantic Oscillation and European climate. *Nature*, **398**, 320–323, https://doi.org/10.1038/18648.

Scaife, A. A., J. R. Knight, G. K. Vallis, and C. K. Folland, 2005: A stratospheric influence on the winter NAO and North Atlantic surface climate. *Geophys. Res. Lett.*, **32**, L18715, https://doi.org/10.1029/2005GL023226.

——, and Coauthors, 2014: Skillful long-range prediction of European and North American winters. *Geophys. Res. Lett.*, **41**, 2514–2519, https://doi.org/10.1002/2014GL059637.

Schaller, N., and Coauthors, 2016: Human influence on climate in the 2014 southern England winter floods and their impacts. *Nat. Climate Change*, **6**, 627–634, https://doi.org/10.1038/nclimate2927.

Simmons, A. J., and D. M. Burridge, 1981: An energy and angular-momentum conserving vertical finite-difference scheme and hybrid vertical coordinates. *Mon. Wea. Rev.*, **109**, 758–766, https://doi.org/10.1175/1520-0493(1981)109<0758:AEAAMC>2.0.CO;2.

Smith, D. M., A. A. Scaife, R. Eade, and J. R. Knight, 2016: Seasonal to decadal prediction of the winter North Atlantic Oscillation: emerging capability and future prospects. *Quart. J. Roy. Meteor. Soc.*, **142**, 611–617, https://doi.org/10.1002/qj.2479.

Sutton, R., and B. Dong, 2012: Atlantic Ocean influence on a shift in European climate in the 1990s. *Nat. Geosci.*, **5**, 788–792, https://doi.org/10.1038/ngeo1595.

Tandon, N. F., E. P. Gerber, A. H. Sobel, and L. M. Polvani, 2013: Understanding Hadley cell expansion versus contraction: Insights from simplified models and implications for recent observations. *J. Climate*, **26**, 4304–4321, https://doi.org/10.1175/JCLI-D-12-00598.1.

Visbeck, M. H., J. W. Hurrell, L. Polvani, and H. M. Cullen, 2001: The North Atlantic Oscillation: Past, present, and future. *Proc. Natl. Acad. Sci. USA*, **98**, 12 876–12 877, https://doi.org/10.1073/pnas.231391598.

Wallace, J. M., and D. S. Gutzler, 1981: Teleconnections in the geopotential height field during the Northern Hemisphere winter. *Mon. Wea. Rev.*, **109**, 784–812, https://doi.org/10.1175/1520-0493(1981)109<0784:TITGHF>2.0.CO;2.

Wang, W., B. T. Anderson, R. K. Kaufmann, and R. B. Myneni, 2004: The relation between the North Atlantic Oscillation and SSTs in the North Atlantic basin. *J. Climate*, **17**, 4752–4759, https://doi.org/10.1175/JCLI-3186.1.

Weisheimer, A., N. Schaller, C. O'Reilly, D. A. MacLeod, and T. Palmer, 2017: Atmospheric seasonal forecasts of the twentieth century: Multi-decadal variability in predictive skill of the winter North Atlantic Oscillation (NAO) and their potential value for extreme event attribution. *Quart. J. Roy. Meteor. Soc.*, **143**, 917–926, https://doi.org/10.1002/qj.2976.

Wilks, D. S., 2011: *Statistical Methods in the Atmospheric Sciences*. 3rd ed. Elsevier, 676 pp.

Woollings, T., A. Hannachi, and B. Hoskins, 2010: Variability of the North Atlantic eddy-driven jet stream. *Quart. J. Roy. Meteor. Soc.*, **136**, 856–868, https://doi.org/10.1002/qj.625.

——, C. Czuchnicki, and C. Franzke, 2014: Twentieth century North Atlantic jet variability. *Quart. J. Roy. Meteor. Soc.*, **140**, 783–791, https://doi.org/10.1002/qj.2197.

Yasunaka, S., and K. Hanawa, 2011: Intercomparison of historical sea surface temperature datasets. *Int. J. Climatol.*, **31**, 1056–1073, https://doi.org/10.1002/joc.2104.